Table 6. List of acquired genomic alterations in chemoresistant ALL samples in comparison with their untreated ALL controls

Sample ID	Chr. region	Start position	End position	CN	Length [Mb]	Candidate genes
ALL3-VCR-R	7q21.2	92155688	92308281	1	0.15	*CDK6*
ALL3-VCR-R	Trisomy 18			3		
ALL17-ARA-C-R	4q13.3	72229564	72258899	0	0.03	*DCK*
ALL17-ARA-C-R	20p13	2026823	2245790	3	0.22	2 genes, *STK35*, *TGM3*
ALL17-ARA-C-R	20p11.21	24662340	24840013	3	0.18	no genes
ALL17-ARA-C-R	20p11.21-20q11.21	24562188	29338325	CNLOH	4.78	20 genes, *ENTPD6*
ALL17-MTX-R	9q31.3-34.11	111124599	130016358	1	18.89	*FPGS*

Chr. = chromosomal; *CN* = copy number; *Mb* = mega–base pair; *R* = resistant.

heterozygous deletion on chromosome 9q encompassing over 50 genes (Fig. 4A). One gene in this newly deleted region was *FPGS*, which is directly involved in methotrexate metabolism [23]. Direct Sanger sequencing of the remaining allele of this gene revealed a newly acquired missense mutation at codon 470 (p.H470R) that was not found in the passage-matched control sample (Fig. 4B). There was no corresponding entry to this variant in the Cosmic database (http://cancer.sanger.ac.uk/cancergenome/projects/cosmic/). According to analysis with PolyPhen-2 (http://genetics.bwh.harvard.edu/pph2/), this mutation was predicted to be possibly damaging with a score of 0.551 (sensitivity: 0.88; specificity: 0.91). Interestingly, there is a registered nonsynonymous SNP in close proximity to this mutation (rs35789560, p.R466C), which has negative effects on the enzyme kinetics [24]. To elucidate whether this mutation was already present at low levels in the untreated control sample, amplicon deep sequencing of this region was performed. Despite reaching twelvethousandfold coverage of the analyzed region, the mutation could not be detected, even at low levels, in the control sample.

Discussion

New, powerful genomic high-throughput techniques, such as genome-wide copy-number analysis using SNP arrays and massive parallel DNA sequencing techniques, allow insights into the heterogeneity of the ALL genome. It is composed, not of a linearly and sequentially developed dominant clone but of a large collection of variable subclonal populations with a complex branching architecture of ancestry as shown here and by others [14,15]. For cancer genomics and therapy, this has the wide-ranging consequence of opening a new avenue to study the specific molecular profiles of disease-founding cell clones.

Existing studies assessing the molecular profiles of ALL relapse samples in comparison with their diagnostic sample have shown that many of the lesions of the relapse clone overlap with lesions of the predominant diagnostic clone, suggesting a common founding origin, but other lesions in the relapse clones differed. In these cases, it was sometimes possible by using sensitive molecular techniques to show that such altered relapse clones were already present in low proportions at diagnosis, suggesting that relapse alterations confer resistance to treatment [1,25,26]. To address mechanisms of resistance acquisition, several strategies have been employed previously, such as whole-exome sequencing approaches of ALL relapse samples versus their diagnosis samples, leading to the identification of activation mutations of drug-inactivating enzymes [27]. Another approach consisted of treating ALL cell lines in vivo to investigate specific pathways involved in drug-induced cell killing such as reversal of glucocorticoid resistance by Akt inhibition [28]. Artificial induction of chemoresistance in ALL cell lines xenografted into immunodeficient mice has been used to test the biological behavior of resistant lines in the setting of graft-versus-leukemia effect [29] or multidrug-resistant mechanisms under treatment with vincristine [30]. However, a targeted analysis of the molecular dynamics of primary ALL cells in vivo under active selection pressure by standard ALL treatment compounds, such as glucocorticoids, vincristine, methotrexate, or cytarabine, has not been performed to our knowledge.

By analysis with high-density SNP arrays of 29 ALL xenografts at different stages of serial transplantation and seven primary patient samples, we confirmed that the ALL xenografts in our study displayed a variegated subclonal branching architecture as shown previously [14,15]. This was evidenced by emergence and clearance of variable clones with different genomic lesions. It was interesting that some lesions, such as *E2A-PBX1* and *ETV6-RUNX1* translocations, were retained in all clones, suggesting that these may be important founder or driver lesions, while other ALL-typical genomic deletions containing *PAX5* or *IKZF1* remained variable, suggesting that these may be dispensable. Although *PAX5* and *IKZF1* could robustly be detected in larger deletions, it is possible that microdeletions of these two genes have been missed in other samples due to relatively low probe coverage on the microarrays for these regions.

Having demonstrated variegated clonal architecture in ALL xenografts, we next showed that the established xenografts could be artificially rendered chemoresistant in vivo against single drugs by repeatedly treating them with standard antileukemic drugs used in the clinic, and thereby we

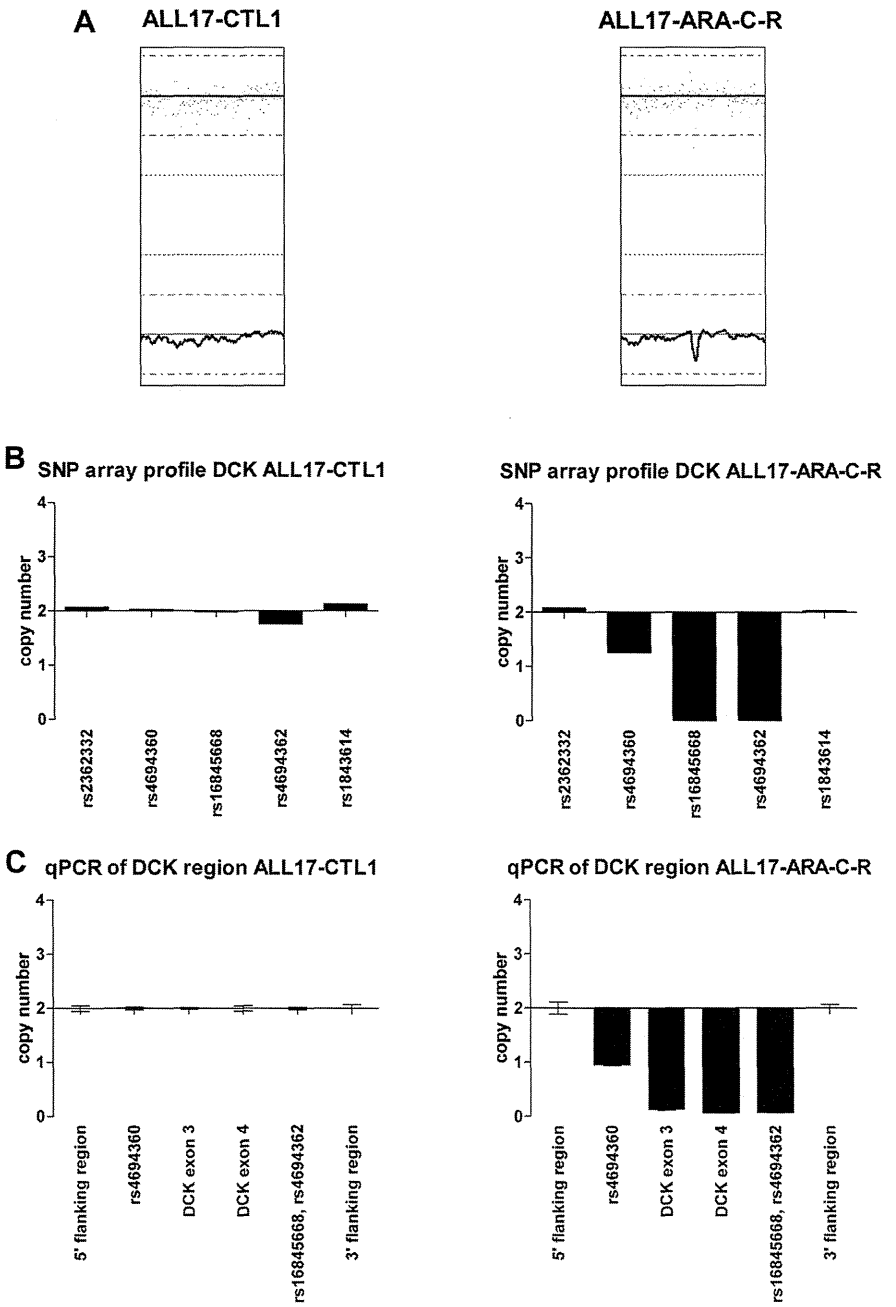

Figure 3. Newly acquired deletion of *DCK* upon in vivo induction of chemoresistance against ARA-C in an ALL xenograft. (**A**) Magnified visualization of copy-number analysis by SNP array of part of chromosome 4q in an untreated ALL xenograft (ALL17-CTL1) and its Ara-C–resistant subclone (ALL17-ARA-C-R) with a new partial homozygous deletion of *DCK*. (**B**) The detection of the deletion is only covered by 3 SNPs on the array, which is why the absolute intensity values of these three SNPs were depicted in separate graphs. These show that, as compared with the untreated ALL control sample (left), *DCK* is heterozygously deleted in the region of the SNP rs4694360 (copy number = 1) and homozygously deleted in the region of the SNPs rs16845668 and rs4694362 (copy number = 0). (**C**) Deletion was validated by quantitative real-time PCR of this region in the untreated sample (left) and the ARA-C resistant sample (right). *AraC* = Cytarabine.

established a new model for studying in vivo chemoresistance. The subsequent copy-number analysis of the xenografted samples showed that there was a trend toward an increased mean number of CNAs in serially passaged xenografts compared with their matched primary patient samples. In the chemoresistant xenografts, the mean number of CNAs was even higher. However, this could also be a reflection of the subtype of the primary leukemia from which these xenografts were derived, since these biopsy samples were not available for a baseline comparison.

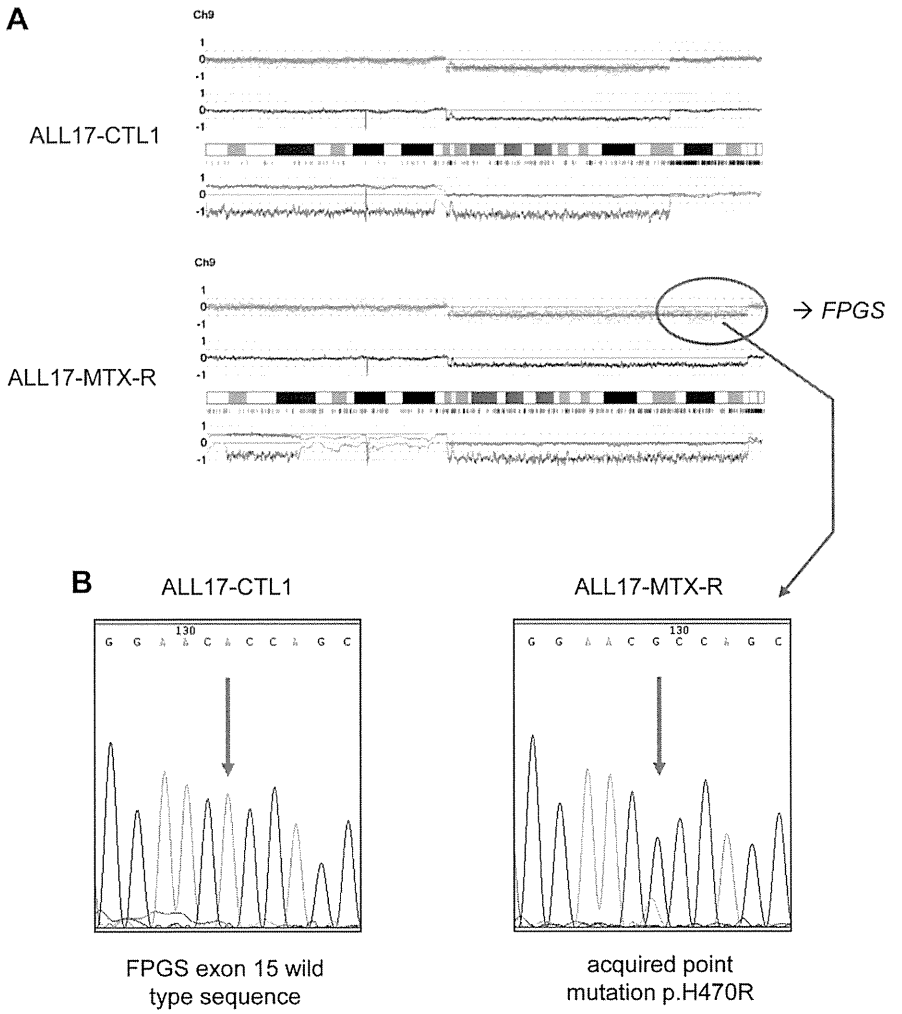

Figure 4. Newly acquired deletion of *FPGS* upon in vivo induction of chemoresistance against MTX in an ALL xenograft. (**A**) Visualization of copy-number analysis by SNP array of chromosome 9 in an untreated ALL xenograft (ALL17-CTL1) and its MTX-resistant subclone (ALL17-MTX-R) with a new telomeric extended heterozygous deletion of the long arm of chromosome 9. (**B**) Sequencing of *FPGS* revealed a newly acquired missense mutation in the remaining allele of *FPGS* in codon 470, putatively leading to a loss of function in the remaining allele of *FPGS*.

Nevertheless, these data are in line with previous results indicating that the procedure of xenografting alone allows for the selection of aggressive subclones already present in the primary diagnostic patient sample, whose molecular profile more closely resembles relapse samples of these patients than the diagnostic sample [31]. This could be a reflection of clonal evolution to adapt to restraints associated with the new xenogeneic microenvironment.

In the data from six pairs of chemoresistant ALL xenografts versus their untreated controls, vincristine-, cytarabine-, and methotrexate-resistant samples displayed newly acquired genomic CNAs, while the dexamethasone-resistant sample did not display any new CNAs. This could perhaps be explained by the far higher genotoxicity of the other three drugs, which are all able to induce increased oxidative stress and DNA breakage [32–34] and may therefore cause an increased occurrence of the observed structural copy-number alterations and DNA breakage as compared with glucocorticoid-induced apoptosis [35]. For the case of vincristine resistance (sample series ALL3), it is unclear how the observed newly acquired genomic changes of a partial *CDK6* deletion and trisomy 18 mediate resistance against the drug. Known mechanisms of resistance against vincristine are limited to observations of a multidrug resistance phenotype, tubulin alterations, and resistance to vincristine-induced apoptosis [36]. Interestingly, the sample pair of ALL3 did not display a genomic deletion of *CDKN2A*. Therefore, the partial deletion of *CDK6* in the vincristine-resistant sample could represent a mechanism of altering cell-cycle regulation to overcome apoptotic signaling induced by vincristine.

In the other two cases of either cytarabine or methotrexate resistance, the newly acquired mechanisms of molecular resistance were more accessible to interpretation.

The cytarabine-resistant cells (xenograft ALL-17) developed a homozygous deletion of the *DCK* gene. Deoxycytidine kinase is an enzyme that catalyzes the initial step of the 5′-phosphorylation of three of the four natural deoxyribonucleosides: deoxycytidine, deoxyguanosine, and deoxyadenosine. Deoxycytidine kinase is also an essential enzyme for the phosphorylation of cytarabine and other nucleoside analogues to their monophosphate forms [37–39]. Disruptions of the function of the *DCK* gene, such as by reduced expression of deoxycytidine kinase, have been associated with resistance to cytarabine [40–42]. To our knowledge, this is the first report of a partial homozygous deletion of *DCK* (exons 3–4) as a mechanism of cytarabine resistance.

The methotrexate-resistant xenograft (ALL17-MTX-R) displayed an enlarged deletion of the long arm of chromosome 9 in comparison to its passage-matched control xenograft. Within the newly acquired deletion is the coding region for the gene *FPGS*, which catalyzes the polyglutamylation of folates and antifolates after uptake into the cell [43,44]. This metabolism creates antifolate polyanions that can no longer be effluxed out of cells, thereby leading to enhanced intracellular retention and increased cytotoxic activity. Therefore, loss of *FPGS* activity is an established mechanism of resistance to antifolates dependent on polyglutamylation in vitro and in vivo [45,46]. Inactivating mutations of *FPGS* have been associated with resistance to antifolate therapy [47,48]. In these previously reported cases, the mutations of *FPGS* were biallelic, implying that the gene function can be rescued by a remaining intact allele if the other one is mutated. The biological effect of the acquired missense mutation H470 R in the *FPGS* gene in our study has not been proven functionally. However, it is highly likely to induce resistance to methotrexate, because neither an extended heterozygous deletion, nor the preexistence of the mutation, even by deep sequencing with greater than twelvethousandfold coverage, could be detected in the passage-matched control sample. Although anecdotal, the circumstance that this mutation could not be detected in the control sample is of special note because, ostensibly, the molecular analysis of artificially rendered chemoresistant subclones of ALL xenografts in this study tested one step further the hypothesis of complex branching clonal architecture in ALL. According to this notion, the mutation should have been detectable in a minor subclone in the diagnostic sample. However, this case emphasizes a second possibility—namely that under the additional pressure of chemotherapy, the genomic variability of ALL cells in vivo is too high even to allow for rapid emergence of new chemoresistant subclones under therapy.

In conclusion, we present a comprehensive genome-wide analysis of pediatric ALL xenografts and confirm recent findings of the complex branching subclonal architecture of ALL. Importantly, we demonstrate for the first time that the model of inducing chemoresistance in xenografted human ALL cells in immunodeficient mice is highly efficient in detecting molecular alterations that confer chemoresistance against established drugs used in the treatment of pediatric ALL. Ultimately, if expanded, this experimental paradigm could be used to catalogue recurrent molecular changes in ALL cells upon induction of chemoresistance. Knowledge of such molecular lesions would, in the future, offer the possibility to prescreen patients with relapse to establish predictive models for response to different relapse therapeutic regimens with the aim of improving clinical outcomes. Moreover, this approach should yield a large number of target genes for development of strategies to circumvent resistance to therapy.

Acknowledgments

Dr D. Nowak has received a research grant from the Deutsche Forschungsgemeinschaft (no. 817/1-1). Prof RB Lock received a Research Fellowship from the National Health and Medical Research Council (Australia). Prof HP Koeffler was supported by the StaR Award (Singapore) and by a National Institutes of Health grant (no. 5R01CA026038-35).

Conflict of interest disclosure

No financial interest/relationships with financial interest relating to the topic of this article have been declared.

References

1. Inaba H, Greaves M, Mullighan CG. Acute lymphoblastic leukaemia. Lancet. 2013;381:1943–1955.
2. Hunger SP, Lu X, Devidas M, et al. Improved survival for children and adolescents with acute lymphoblastic leukemia between 1990 and 2005: A report from the children's oncology group. J Clin Oncol. 2012;30:1663–1669.
3. Bachmann PS, Lock RB. In vivo models of childhood leukemia for preclinical drug testing. Curr Drug Targets. 2007;8:773–783.
4. Lee EM, Bachmann PS, Lock RB. Xenograft models for the preclinical evaluation of new therapies in acute leukemia. Leuk Lymphoma. 2007;48:659–668.
5. Liem NL, Papa RA, Milross CG, et al. Characterization of childhood acute lymphoblastic leukemia xenograft models for the preclinical evaluation of new therapies. Blood. 2004;103:3905–3914.
6. Bonnet D, Dick JE. Human acute myeloid leukemia is organized as a hierarchy that originates from a primitive hematopoietic cell. Nat Med. 1997;3:730–737.
7. Lapidot T, Sirard C, Vormoor J, et al. A cell initiating human acute myeloid leukaemia after transplantation into SCID mice. Nature. 1994;367:645–648.
8. Kawamata N, Ogawa S, Zimmermann M, et al. Molecular allelokaryotyping of pediatric acute lymphoblastic leukemias by high-resolution single nucleotide polymorphism oligonucleotide genomic microarray. Blood. 2008;111:776–784.
9. Mullighan CG, Goorha S, Radtke I, et al. Genome-wide analysis of genetic alterations in acute lymphoblastic leukaemia. Nature. 2007;446:758–764.
10. Mullighan CG, Miller CB, Radtke I, et al. BCR-ABL1 lymphoblastic leukaemia is characterized by the deletion of Ikaros. Nature. 2008;453:110–114.

11. Mullighan CG, Su X, Zhang J, et al. Deletion of IKZF1 and prognosis in acute lymphoblastic leukemia. N Engl J Med. 2009;360:470–480.
12. Okamoto R, Ogawa S, Nowak D, et al. Genomic profiling of adult acute lymphoblastic leukemia by single nucleotide polymorphism oligonucleotide microarray and comparison to pediatric acute lymphoblastic leukemia. Haematologica. 2010;95:1481–1488.
13. Shlush LI, Zandi S, Mitchell A, et al. Identification of pre-leukaemic haematopoietic stem cells in acute leukaemia. Nature. 2014;506:328–333.
14. Anderson K, Lutz C, van Delft FW, et al. Genetic variegation of clonal architecture and propagating cells in leukaemia. Nature. 2011;469: 356–361.
15. Notta F, Mullighan CG, Wang JC, et al. Evolution of human BCR-ABL1 lymphoblastic leukaemia-initiating cells. Nature. 2011;469: 362–367.
16. Lock RB, Liem N, Farnsworth ML, et al. The nonobese diabetic/ severe combined immunodeficient (NOD/SCID) mouse model of childhood acute lymphoblastic leukemia reveals intrinsic differences in biologic characteristics at diagnosis and relapse. Blood. 2002;99: 4100–4108.
17. Bachmann PS, Gorman R, Papa RA, et al. Divergent mechanisms of glucocorticoid resistance in experimental models of pediatric acute lymphoblastic leukemia. Cancer Res. 2007;67:4482–4490.
18. High LM, Szymanska B, Wilczynska-Kalak U, et al. The Bcl-2 homology domain 3 mimetic ABT-737 targets the apoptotic machinery in acute lymphoblastic leukemia resulting in synergistic in vitro and in vivo interactions with established drugs. Mol Pharmacol. 2010; 77:483–494.
19. Szymanska B, Wilczynska-Kalak U, Kang MH, et al. Pharmacokinetic modeling of an induction regimen for in vivo combined testing of novel drugs against pediatric acute lymphoblastic leukemia xenografts. PLoS One. 2012;7:e33894.
20. Nannya Y, Sanada M, Nakazaki K, et al. A robust algorithm for copy number detection using high-density oligonucleotide single nucleotide polymorphism genotyping arrays. Cancer Res. 2005;65:6071–6079.
21. Yamamoto G, Nannya Y, Kato M, et al. Highly sensitive method for genomewide detection of allelic composition in nonpaired, primary tumor specimens by use of affymetrix single-nucleotide-polymorphism genotyping microarrays. Am J Hum Genet. 2007;81:114–126.
22. Livak KJ, Schmittgen TD. Analysis of relative gene expression data using real-time quantitative PCR and the 2(-Delta Delta C(T)) method. Methods. 2001;25:402–408.
23. Synold TW, Willits EM, Barredo JC. Role of folylpolygutamate synthetase (FPGS) in antifolate chemotherapy; a biochemical and clinical update. Leuk Lymphoma. 1996;21:9–15.
24. Leil TA, Endo C, Adjei AA, et al. Identification and characterization of genetic variation in the folylpolyglutamate synthase gene. Cancer Res. 2007;67:8772–8782.
25. Mullighan CG, Phillips LA, Su X, et al. Genomic analysis of the clonal origins of relapsed acute lymphoblastic leukemia. Science. 2008;322:1377–1380.
26. Yang JJ, Bhojwani D, Yang W, et al. Genome-wide copy number profiling reveals molecular evolution from diagnosis to relapse in childhood acute lymphoblastic leukemia. Blood. 2008;112:4178–4183.
27. Tzoneva G, Perez-Garcia A, Carpenter Z, et al. Activating mutations in the NT5C2 nucleotidase gene drive chemotherapy resistance in relapsed ALL. Nat Med. 2013;19:368–371.
28. Piovan E, Yu J, Tosello V, et al. Direct reversal of glucocorticoid resistance by AKT inhibition in acute lymphoblastic leukemia. Cancer Cell. 2013;24:766–776.
29. Jansson J, Hsu YC, Kuzin II, Campbell A, Mullen CA. Acute lymphoblastic leukemia cells that survive combination chemotherapy in vivo remain sensitive to allogeneic immune effects. Leuk Res. 2011; 35:800–807.
30. Zunino SJ, Storms DH, Ducore JM. Novel in vivo model of inducible multi-drug resistance in acute lymphoblastic leukemia with chromosomal translocation t(4;11). Cancer lett. 2010;296:49–54.
31. Clappier E, Gerby B, Sigaux F, et al. Clonal selection in xenografted human T cell acute lymphoblastic leukemia recapitulates gain of malignancy at relapse. J Exp Med. 2011;208:653–661.
32. Grant S. Ara-C: Cellular and molecular pharmacology. Adv Cancer Res. 1998;72:197–233.
33. Jiang W, Lu Y, Chen Z, et al. Studying the genotoxicity of vincristine on human lymphocytes using comet assay, micronucleus assay and TCR gene mutation test in vitro. Toxicology. 2008;252:113–117.
34. Martin SA, McCarthy A, Barber LJ, et al. Methotrexate induces oxidative DNA damage and is selectively lethal to tumour cells with defects in the DNA mismatch repair gene MSH2. EMBO Molecular Medicine. 2009;1:323–337.
35. Schlossmacher G, Stevens A, White A. Glucocorticoid receptor-mediated apoptosis: Mechanisms of resistance in cancer cells. J Endocrinol. 2011;211:17–25.
36. Gidding CE, Kellie SJ, Kamps WA, de Graaf SS. Vincristine revisited. Crit Rev Oncol Hematol. 1999;29:267–287.
37. Bouffard DY, Laliberte J, Momparler RL. Kinetic studies on 2',2'-difluorodeoxycytidine (Gemcitabine) with purified human deoxycytidine kinase and cytidine deaminase. Biochem Pharmacol. 1993;45: 1857–1861.
38. Carson DA, Wasson DB, Kaye J, et al. Deoxycytidine kinase-mediated toxicity of deoxyadenosine analogs toward malignant human lymphoblasts in vitro and toward murine L1210 leukemia in vivo. Proc Natl Acad Sci U S A. 1980;77:6865–6869.
39. Fernandez-Calotti P, Jordheim LP, Giordano M, Dumontet C, Galmarini CM. Substrate cycles and drug resistance to 1-beta-D-arabinofuranosylcytosine (araC). Leuk Lymphoma. 2005;46:335–346.
40. Kanno S, Hiura T, Ohtake T, et al. Characterization of resistance to cytosine arabinoside (Ara-C) in NALM-6 human B leukemia cells. Clin Chim Acta. 2007;377:144–149.
41. Sarkar M, Han T, Damaraju V, Carpenter P, Cass CE, Agarwal RP. Cytosine arabinoside affects multiple cellular factors and induces drug resistance in human lymphoid cells. Biochem Pharmacol. 2005;70:426–432.
42. Song JH, Kim SH, Kweon SH, Lee TH, Kim HJ, Kim TS. Defective expression of deoxycytidine kinase in cytarabine-resistant acute myeloid leukemia cells. Int J Oncol. 2009;34:1165–1171.
43. McGuire JJ, Hsieh P, Coward JK, Bertino JR. Enzymatic synthesis of folylpolyglutamates. Characterization of the reaction and its products. J Biol Chem. 1980;255:5776–5788.
44. Poser RG, Sirotnak FM, Chello PL. Differential synthesis of methotrexate polyglutamates in normal proliferative and neoplastic mouse tissues in vivo. Cancer Res. 1981;41:4441–4446.
45. Liani E, Rothem L, Bunni MA, Smith CA, Jansen G, Assaraf YG. Loss of folylpoly-gamma-glutamate synthetase activity is a dominant mechanism of resistance to polyglutamylation-dependent novel antifolates in multiple human leukemia sublines. Int J Cancer. 2003;103: 587–599.
46. Stark M, Wichman C, Avivi I, Assaraf YG. Aberrant splicing of folylpolyglutamate synthetase as a novel mechanism of antifolate resistance in leukemia. Blood. 2009;113:4362–4369.
47. Leclerc GJ, York TA, Hsieh-Kinser T, Barredo JC. Molecular basis for decreased folylpoly-gamma-glutamate synthetase expression in a methotrexate resistant CCRF-CEM mutant cell line. Leuk Res. 2007;31:293–299.
48. Zhao R, Titus S, Gao F, Moran RG, Goldman ID. Molecular analysis of murine leukemia cell lines resistant to 5, 10-dideazatetrahydrofolate identifies several amino acids critical to the function of folylpolyglutamate synthetase. J Biol Chem. 2000;275:26599–26606.

the L205R mutation enhanced the phosphorylation catalysis of PKA.

The identification of activating mutations in oncogenes is particularly valuable in developing targeted therapies for cancer. PKA signaling plays a pivotal role in various physiological and pathological processes, including development, metabolism, and tumorigenesis. Although inactivating mutations in *PRKAR1A* and phosphodiesterase genes are known in adrenal hyperplasia, we revealed the activating *PRKACA* L205R mutation and several potential functional mutated genes in ACTs. Future investigations on mutagenesis and hormones or environmental initiators of the L205R mutation may provide clues for prevention or treatment of Cushing's syndrome.

REFERENCES AND NOTES

1. J. Newell-Price, X. Bertagna, A. B. Grossman, L. K. Nieman, *Lancet* **367**, 1605–1617 (2006).
2. C. A. Stratakis, S. A. Boikos, *Nat. Clin. Pract. Endocrinol. Metab.* **3**, 748–757 (2007).
3. L. S. Kirschner *et al.*, *Nat. Genet.* **26**, 89–92 (2000).
4. See supplementary materials on *Science* Online.
5. A. Berthon, A. Martinez, J. Bertherat, P. Val, *Mol. Cell. Endocrinol.* **351**, 87–95 (2012).
6. S. Gaujoux *et al.*, *Clin. Cancer Res.* **16**, 5133–5141 (2010).
7. L. S. Weinstein *et al.*, *N. Engl. J. Med.* **325**, 1688–1695 (1991).
8. M. C. Fragoso *et al.*, *J. Clin. Endocrinol. Metab.* **88**, 2147–2151 (2003).
9. J. Min, Q. Feng, Z. Li, Y. Zhang, R.-M. Xu, *Cell* **112**, 711 (2003).
10. Y. Okada *et al.*, *Cell* **121**, 167–178 (2005).
11. G. Assié *et al.*, *N. Engl. J. Med.* **369**, 2105–2114 (2013).
12. N. Galjart, *Nat. Rev. Mol. Cell Biol.* **6**, 487–498 (2005).
13. M. D. Uhler *et al.*, *Proc. Natl. Acad. Sci. U.S.A.* **83**, 1300–1304 (1986).
14. B. Nolen, S. Taylor, G. Ghosh, *Mol. Cell* **15**, 661–675 (2004).
15. P. Madhusudan, P. Akamine, N. H. Xuong, S. S. Taylor, *Nat. Struct. Biol.* **9**, 273–277 (2002).
16. M. J. Moore, J. A. Adams, S. S. Taylor, *J. Biol. Chem.* **278**, 10613–10618 (2003).
17. J. Yang, L. F. Ten Eyck, N. H. Xuong, S. S. Taylor, *J. Mol. Biol.* **336**, 473–487 (2004).
18. J. Yang *et al.*, *J. Mol. Biol.* **346**, 191–201 (2005).
19. C. Kim, N. H. Xuong, S. S. Taylor, *Science* **307**, 690–696 (2005).
20. C. Kim, C. Y. Cheng, S. A. Saldanha, S. S. Taylor, *Cell* **130**, 1032–1043 (2007).
21. D. Sarkar *et al.*, *J. Clin. Endocrinol. Metab.* **86**, 1653–1659 (2001).
22. S. Acharyya *et al.*, *Cell* **150**, 165–178 (2012).
23. E. Meimaridou *et al.*, *Endocr. Dev.* **24**, 57–66 (2013).
24. D. Lin *et al.*, *Science* **267**, 1828–1831 (1995).
25. P. R. Manna, M. T. Dyson, D. M. Stocco, *Mol. Hum. Reprod.* **15**, 321–333 (2009).
26. S. S. Taylor, R. Ilouz, P. Zhang, A. P. Kornev, *Nat. Rev. Mol. Cell Biol.* **13**, 646–658 (2012).

ACKNOWLEDGMENTS

Supported by Natural Science Foundation of China grants 30900702, 81130016, and 81270859, and by Guangdong Innovative Research Team Program grant 2009010016. The sequencing data have been deposited in the European Genome-phenome Archive (accession no. EGAS00001000712).

SUPPLEMENTARY MATERIALS

www.sciencemag.org/content/344/6186/913/suppl/DC1
Materials and Methods
Figs. S1 to S8
Tables S1 to S11
References (*27–40*)

9 December 2013; accepted 21 March 2014
Published online 3 April 2014;
10.1126/science.1249480

CANCER GENOMICS

Recurrent somatic mutations underlie corticotropin-independent Cushing's syndrome

Yusuke Sato,[1,2]* Shigekatsu Maekawa,[2]* Ryohei Ishii,[3] Masashi Sanada,[1] Teppei Morikawa,[4] Yuichi Shiraishi,[5] Kenichi Yoshida,[1] Yasunobu Nagata,[1] Aiko Sato-Otsubo,[1] Tetsuichi Yoshizato,[1] Hiromichi Suzuki,[1] Yusuke Shiozawa,[1] Keisuke Kataoka,[1] Ayana Kon,[1] Kosuke Aoki,[1] Kenichi Chiba,[5] Hiroko Tanaka,[6] Haruki Kume,[2] Satoru Miyano,[5,6] Masashi Fukayama,[4] Osamu Nureki,[3] Yukio Homma,[2]† Seishi Ogawa[1]†

Cushing's syndrome is caused by excess cortisol production from the adrenocortical gland. In corticotropin-independent Cushing's syndrome, the excess cortisol production is primarily attributed to an adrenocortical adenoma, in which the underlying molecular pathogenesis has been poorly understood. We report a hotspot mutation (L206R) in *PRKACA*, which encodes the catalytic subunit of cyclic adenosine monophosphate (cAMP)–dependent protein kinase (PKA), in more than 50% of cases with adrenocortical adenomas associated with corticotropin-independent Cushing's syndrome. The L206R PRKACA mutant abolished its binding to the regulatory subunit of PKA (PRKAR1A) that inhibits catalytic activity of PRKACA, leading to constitutive, cAMP-independent PKA activation. These results highlight the major role of cAMP-independent activation of cAMP/PKA signaling by somatic mutations in corticotropin-independent Cushing's syndrome, providing insights into the diagnosis and therapeutics of this syndrome.

Cushing's syndrome is a systemic disorder associated with various constitutive symptoms—such as hypertension, impaired glucose tolerance, central obesity, osteoporosis, and depression—that are ascribed to cortisol overproduction (*1–3*). Cortisol biosynthesis is primarily regulated by corticotropin secreted from the anterior pituitary gland. Corticotropin acts by binding to the melanocortin-2 receptor, increases cyclic adenosine monophosphate (cAMP) production, and activates cAMP-dependent protein kinase [protein kinase A (PKA)] (*4*). While aberrant corticotropin secretion from pituitary adenoma or other ectopic sites is the leading cause of Cushing's syndrome (corticotropin-dependent Cushing's syndrome), excess cortisol is autonomously produced by adrenocortical tumors in patients with corticotropin-independent Cushing's syndrome (*2, 5, 6*). Although mutations in the regulatory subunit type I alpha of PKA (*PRKAR1A*) (*7, 8*) guanine nucleotide-binding protein subunit alpha (*GNAS*) (*9*), phosphodiesterase-8B (*PDE8B*) (*10, 11*) and -11A (*PDE11A*) (*12*), and armadillo repeat containing 5 (*ARMC5*) (*13*) are responsible for rare syndromic or hereditary disorders with bilateral adrenocortical hyperplasia, molecular pathogenesis of cortisol-producing adrenocortical adenomas, which account for a large portion of corticotropin-independent Cushing's syndrome (*6*), are less studied.

To investigate genetic lesions in corticotropin-independent Cushing's syndrome, we performed whole-exome sequencing (WES) of eight adrenocortical tumors and matched normal specimens (fig. S1 and table S1). We identified a total of 45 validated nonsynonymous and 59 putative synonymous somatic mutations (tables S2 and S3) (see the supplementary materials). Remarkably, the gene encoding the catalytic subunit (C subunit) of PKA (*PRKACA*) was recurrently mutated in four out of the eight cases, resulting in an identical c.T617G mutation predicted to cause a conversion of leucine to arginine at amino acid position 206 (p.L206R). Together with a *GNAS* mutation (p.R201C), five of the eight cases had somatic mutations in genes involved in the cAMP/PKA signaling pathway. No allelic imbalances were observed at both gene loci in single-nucleotide polymorphism (SNP) array analysis (fig. S2), indicating that these mutations were heterozygous, which was consistent with the observation that, in exome sequencing, variant allele frequencies (VAF) of *PRKACA/GNAS* mutations were comparable to those of other somatic mutations (fig. S3). Mutations were not detected in any other known causative genes, including *PRKAR1A*, *PDE11A*, *PDE8B*, and *ARMC5*.

[1]Department of Pathology and Tumor Biology, Graduate School of Medicine, Kyoto University, Kyoto, Japan. [2]Department of Urology, Graduate School of Medicine, The University of Tokyo, Tokyo, Japan. [3]Department of Biophysics and Biochemistry, Graduate School of Science, The University of Tokyo, Tokyo, Japan. [4]Department of Pathology, Graduate School of Medicine, The University of Tokyo, Tokyo, Japan. [5]Laboratory of DNA Information Analysis, Human Genome Center, Institute of Medical Science, The University of Tokyo, Tokyo, Japan. [6]Laboratory of Sequence Analysis, Human Genome Center, Institute of Medical Science, The University of Tokyo, Tokyo, Japan.
*These authors contributed equally to this work. †Corresponding author. E-mail: sogawa-tky@umin.ac.jp (S.O.); homma-uro@umin.ac.jp (Y.H.)

We performed follow-up sequencing of *PRKACA* and *GNAS* as well as previously reported genes (*PRKAR1A*, *PDE11A*, *PDE8B*, and *ARMC5*) in an additional 57 cases (see the supplementary materials). The L206R mutation in *PRKACA* was found in 30 out of the 57 follow-up cases, of which 24 cases were confirmed as being somatic, whereas *GNAS* mutations were found in 10 cases, with somatic origin being confirmed in six cases (table S1, Fig. 1, and fig. S4). No mutations were found in the previously reported genes. The eight samples double-negative for *PRKACA* and *GNAS* mutations were tested for mutations in seven additional genes that were mutated and expressed in three double-negative exome cases, but no more recurrent mutations were identified. Combined with the four *PRKACA* and one *GNAS* mutations in the discovery cases, *PRKACA* and *GNAS* were mutated in 34 (52.3%) and 11 (16.9%) out of the 65 cases with corticotropin-independent Cushing's syndrome, respectively, where both mutations were completely mutually exclusive (Fisher's exact test, $P = 9.46 \times 10^{-5}$) (Fig. 1). The somatic origin was confirmed for 28 out of 28 *PRKACA* and 6 out of 6 *GNAS* mutations thus far tested. In addition, VAFs of *PRKACA* and *GNAS* mutations in deep sequencing were distributed between 0.08 and 0.35, whereas those of most heterozygous SNPs (83%) were between 0.4 and 0.6 (fig. S5), indicating that most of these mutations were somatic in origin.

Patients with mutated *PRKACA* showed significantly higher cortisol levels on the 1-mg dexamethasone suppression test (DST) compared with wild-type *PRKACA* and *GNAS* (*t* test, $P = 2.60 \times 10^{-3}$) (Fig. 2A). *PRKACA*-mutated adenomas had a significantly smaller tumor diameter than those with no known mutations (*t* test, $P = 4.93 \times 10^{-5}$) (Fig. 2B), suggesting that *PRKACA*-mutated adenomas may have higher cortisol production. *GNAS*-mutated adenomas also showed higher cortisol levels on 1-mg DST and have a smaller tumor size. Seventy-six percent of the patients with clinical Cushing's syndrome had a mutation of either gene, whereas only two of nine patients with subclinical Cushing's syndrome had mutated *PRKACA* or *GNAS* genes (Fisher's exact test, $P = 2.87 \times 10^{-3}$) (Fig. 2C and table S4), indicating that these mutations were enriched for clinical Cushing's syndrome.

PRKACA is the catalytic (C) subunit of the tetrameric PKA holoenzyme, which binds tissue-specific dimeric regulatory (R) subunits (*14*–*16*). In the native state, the C subunit is kept inactivated through the binding of the R subunit, which masks the catalytic site of the C subunit (Fig. 3A). However, when intracellular cAMP is up-regulated by external stimuli, each R subunit binds two cAMP molecules, which causes a conformational change in the R subunit to promote dissociation of the C subunit from the PKA complex (*14*–*16*), allowing for the translocation of the dissociated, and thereby activated, free C subunit to the nucleus and phosphorylation of its target substrates therein (*17*, *18*). The highly conserved L206 residue of PRKACA, which resides within the P+1 loop of the C subunit, lies on the surface of the large lobe of PRKACA and is thought to be essential for the catalytic activity of the kinase (Fig. 3A, and fig. S6) (*14*–*16*). In the absence of cAMP, the inhibitory region of the R subunit docks to the active site cleft of the C subunit, including the P+1 loop. The L206 residue is located at the interface between the C subunit and the inhibitory region in the R subunit to form a hydrophobic interaction with the I99 residue of the R subunit (Fig. 3B). Thus, the substitution from the small hydrophobic leucine to a large hydrophobic arginine is predicted to cause steric hindrance and abolish the binding of the C and R subunits (Fig. 3C), resulting in constitutive, cAMP-independent activation of PKA.

In fact, when the PKA complex was reconstituted in vitro using purified proteins (fig. S7), PRKAR1A binds the wild-type C subunit and suppresses its PKA activity in the absence of cAMP, and the suppression is recovered in the presence of cAMP with substantially reduced interaction with the wild-type C subunit (Fig. 4, A and B). In contrast, the R subunit can no longer bind the L206R PRKACA mutant with constitutive PKA activation, regardless of the presence or absence of cAMP (Fig. 4, A and B). The loss of binding to the R subunit and consequent cAMP-independent PKA activation for the mutant PRKACA was also demonstrated in vivo. When expressed in human embryonic kidney 293T (HEK293T) cells (fig. S8), wild-type PRKACA, but not the L206R PRKACA mutant, coimmunoprecipitated with PRKAR1A (Fig. 4C). Both mock- and wild-type *PRKACA*-transduced cells showed increased PKA activity accompanied by an elevated phosphorylation of cAMP response element–binding protein (pCREB), one of the major downstream targets of PKA activation (Fig. 4, D and E, and fig. S9), on cAMP induction by forskolin treatment (see the supplementary materials), whereas mutant *PRKACA*-transduced cells demonstrated a higher basal level of PKA activity and CREB phosphorylation, regardless of forskolin treatment (Fig. 4, D and E, and fig. S9). To confirm the cAMP-independent activation of the mutant PRKACA, we examined the effect of two PRKACA inhibitors (H89 and KT5720) and a competitive inhibitor of cAMP binding for the R subunit (Rp-cAMPS) on the activity of the L206R mutant (see the supplementary materials). PKA activation in the L206R mutant–transduced cells in the absence of forskolin was suppressed by H89 and KT5720 (*t* test, $P = 1.60 \times 10^{-3}$ and $P = 1.86 \times 10^{-3}$, respectively) but not in Rp-cAMPS–treated cells, supporting further that the consequence of the L206R mutation is constitutive, cAMP-independent activation of PKA (Fig. 4F and fig. S10).

Finally, as predicted from low stability of free C subunits, primary *PRKACA*-mutated tumors showed significantly lower PRKACA protein expression compared with unmutated tumors (*t* test, $P = 5.70 \times 10^{-3}$) and normal adrenocortical tissues (*t* test, $P = 2.09 \times 10^{-2}$) (Fig. 4G and fig. S11), although no significant difference was observed for downstream signaling, such as pCREB or steroidogenic acute regulatory protein (StAR). The reduced intracellular expression of the mutant PRKACA protein was also observed for

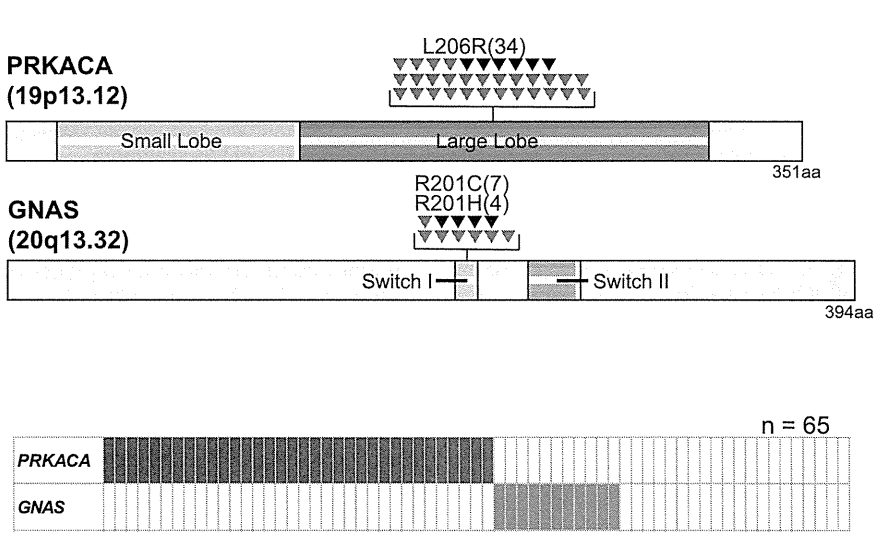

Fig. 1. Recurrent mutations in *PRKACA* and *GNAS*. (**A**) Mutations in *PRKACA* (top) and *GNAS* (bottom) identified in 65 patients with corticotropin-independent Cushing's syndrome (arrowheads). Confirmed somatic mutations are indicated in red. (**B**) Mutually exclusive distribution of *PRKACA* and *GNAS* mutations.

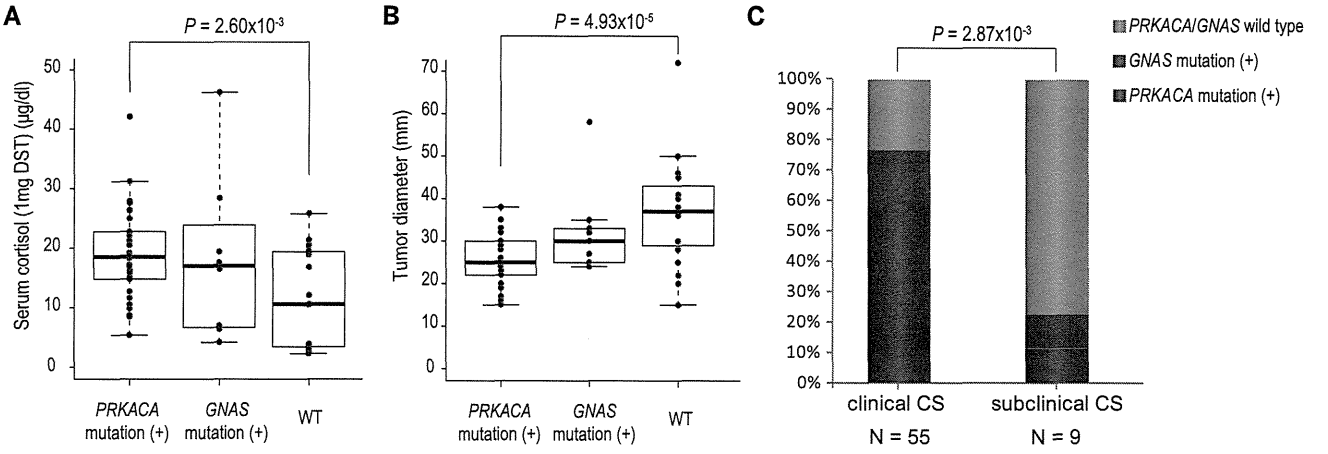

Fig. 2. Relationship between mutation status and clinical features. (**A** and **B**) Serum cortisol level of 1-mg dexamethasone (A) and the diameter of adrenocortical adenoma (B) according to the mutation status of *PRKACA*/*GNAS* genes. (**C**) Clinical and subclinical Cushing's syndrome as attributed to mutated *PRKACA*, *GNAS*, or other, currently undetected, cause.

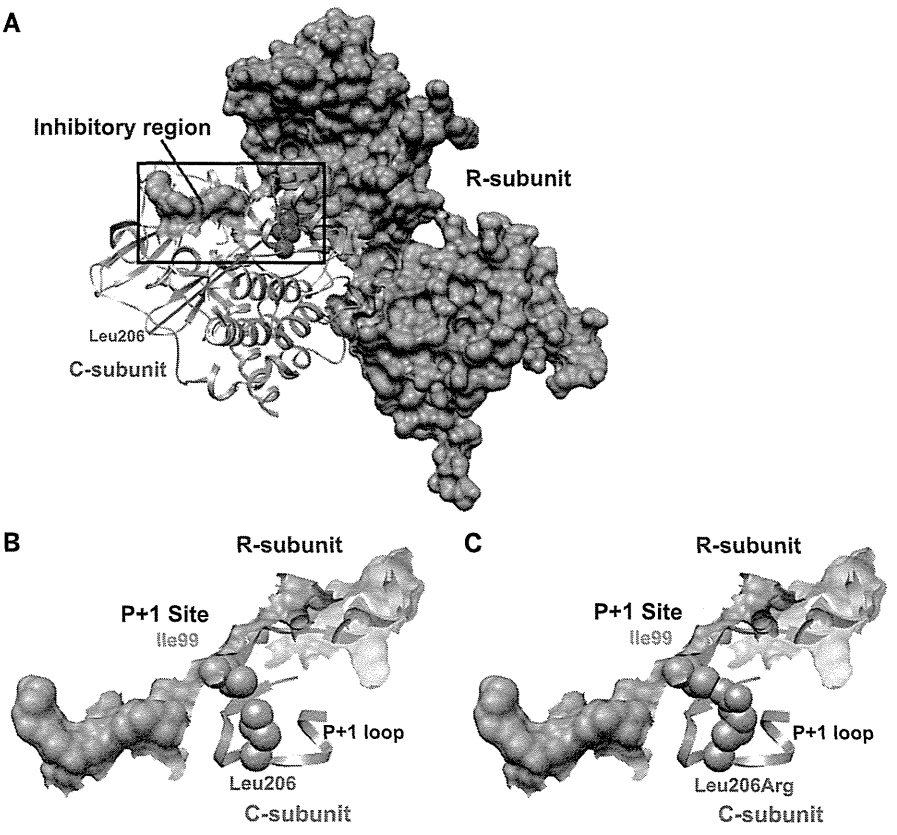

Fig. 3. Effect of L206R mutation on three-dimensional structures of PKA. (**A**) Three-dimensional structure of the PKA complex, composed of C (PRKACA) (pink) and R (PRKAR1A) (cyan) subunits, is depicted using the University of California–San Francisco Chimera program, based on the Research Collaboratory for Structural Bioinformatics Protein Data Bank (PDB ID: 2QCS). L206 is shown in red. (**B** and **C**) A predicted effect of the L206R mutation within the P+1 loop on the interaction with the R subunit (C) in comparison with wild-type PRKACA (B).

exogenously introduced PRKACA in different cell types (Fig. 4H and fig. S12). However, compared with the wild-type protein, mutant PRKACA was more enriched in the nuclear than in the cytoplasmic fraction (Fig. 4H).

In conclusion, frequent somatic mutations in *PRKACA* and *GNAS* genes underlie corticotropin-independent Cushing's syndrome (fig. S13). Strikingly, in accordance with a recent report (*19*) *PRKACA* mutations were found in more than 50% of the current cohort. All the mutations were the identical L206R substitution, which prevents binding to the inhibitory R subunits and results in constitutive, cAMP-independent activation of PKA. *GNAS* mutations were also detected in a substantial fraction of the present cohort (11/65 or 16.9%), in which all were confined to the R201 residue. Steroid hormone biosynthesis in steroidogenic cells is primarily regulated through activation of the cAMP/PKA signaling pathway (*20*). *PRKACA* and *GNAS* mutations in adrenocortical cells affecting this pathway are thus a likely factor responsible for the excessive production of cortisol and together account for as many as 70% of the current cohort of the patients. In contrast, the remaining 30% of the patients with no mutations in either gene tended to show lower cortisol levels on 1-mg DST and had a larger tumor size compared with *PRKACA*-mutated patients. In addition, the identified mutations were confined almost exclusively to patients with clinical Cushing's syndrome, suggesting that double-negative cases have distinct pathogenesis, with driver mutations still to be identified. It should be warranted to identify the genetic basis of double-negative cases in future studies.

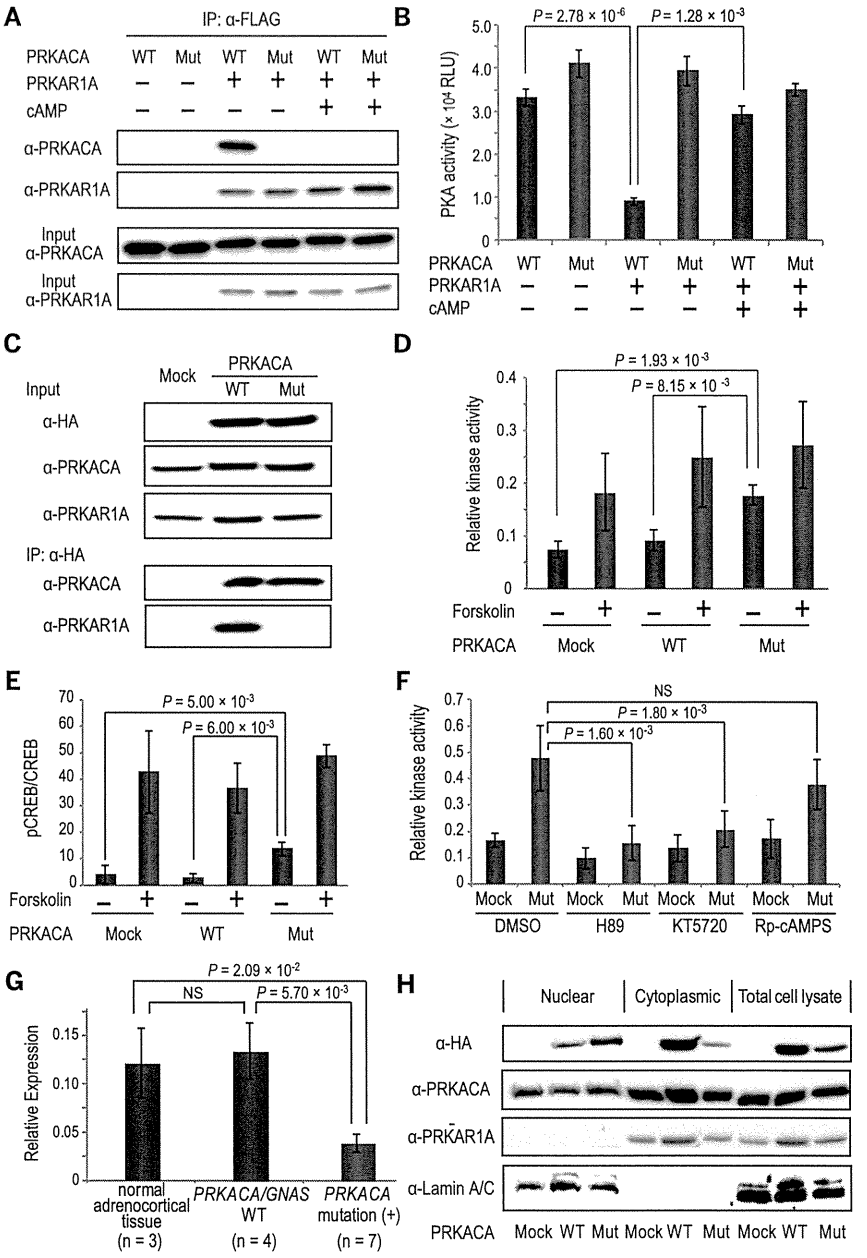

Fig. 4. Functional characterization of PRKACA mutant. (**A**) Immunoblot analysis of antibody to FLAG immunoprecipitates of the PKA reconstructed in vitro with large-scale–purified proteins, in which PRKACA and PRKAR1A subunits are tagged with hemagglutinin (HA) and FLAG, respectively. (**B**) In vitro PKA activities of wild-type and mutant PRKACA in the presence or absence of PRKAR1A and cAMP with purified proteins. (**C**) Immunoblot analysis of the total cell lysates (input) and antibody to HA immunoprecipitates from HEK293T cells stably transduced with either mock, wild-type, or mutant PRKACA tagged with HA with indicated antibodies. (**D**) PKA activities in HEK293T cells stably transduced with either mock, wild-type, or mutant PRKACA in the presence or absence of forskolin stimulation. (**E**) Relative expression of pCREB to total CREB in HEK293T cells stably transduced with either mock, wild-type, or mutant PRKACA as determined by densitometry of the immunoblots. (**F**) The effect of inhibition of PKA (H89 and KT5720) and cAMP (Rp-cAMPS) in HEK293T cells transduced with mock or mutant PRKACA. (**G**) PRKACA expression standardized for mRNA expression in *PRKACA*-mutated and unmutated adenomas and matched normal adrenocortical tissues. (**H**) Western blot analysis of indicated fractions of cell lysates from wild-type and mutant PRKACA-transduced HEK293T cells using indicated antibodies. Standard errors and significant differences are indicated [(C) to (G)].

REFERENCES AND NOTES

1. L. K. Nieman *et al.*, *J. Clin. Endocrinol. Metab.* **93**, 1526–1540 (2008).
2. B. A. Hatipoglu, *J. Surg. Oncol.* **106**, 565–571 (2012).
3. J. Newell-Price, X. Bertagna, A. B. Grossman, L. K. Nieman, *Lancet* **367**, 1605–1617 (2006).
4. K. G. Mountjoy, L. S. Robbins, M. T. Mortrud, R. D. Cone, *Science* **257**, 1248–1251 (1992).
5. D. N. Orth, *N. Engl. J. Med.* **332**, 791–803 (1995).
6. C. A. Stratakis, *Endocr. Dev.* **13**, 117–132 (2008).
7. L. S. Kirschner *et al.*, *Nat. Genet.* **26**, 89–92 (2000).
8. L. S. Kirschner *et al.*, *Hum. Mol. Genet.* **9**, 3037–3046 (2000).
9. L. S. Weinstein *et al.*, *N. Engl. J. Med.* **325**, 1688–1695 (1991).
10. A. Horvath *et al.*, *Nat. Genet.* **38**, 794–800 (2006).
11. A. Horvath *et al.*, *Cancer Res.* **66**, 11571–11575 (2006).
12. A. Horvath, V. Mericq, C. A. Stratakis, *N. Engl. J. Med.* **358**, 750–752 (2008).
13. G. Assié *et al.*, *N. Engl. J. Med.* **369**, 2105–2114 (2013).
14. M. J. Moore, J. A. Adams, S. S. Taylor, *J. Biol. Chem.* **278**, 10613–10618 (2003).
15. C. Kim, N. H. Xuong, S. S. Taylor, *Science* **307**, 690–696 (2005).
16. C. Kim, C. Y. Cheng, S. A. Saldanha, S. S. Taylor, *Cell* **130**, 1032–1043 (2007).
17. M. R. Montminy, L. M. Bilezikjian, *Nature* **328**, 175–178 (1987).
18. A. T. Harootunian *et al.*, *Mol. Biol. Cell* **4**, 993–1002 (1993).
19. F. Beuschlein *et al.*, *N. Engl. J. Med.* **370**, 1019–1028 (2014).
20. A. M. Lefrancois-Martinez *et al.*, *J. Biol. Chem.* **286**, 32976–32985 (2011).

ACKNOWLEDGMENTS

We thank Y. Mori, M. Nakamura, N. Mizota, S. Ichimura, and M. Yamakawa for their technical assistance. The retroviral vector, pGCDNsamIRES-EGFP, was kindly provided by M. Onodera (National Research Institute for Child Health and Development). This work was supported by the Japan Society for the Promotion of Science (JSPS) through Grants-in-Aid for Scientific Research (KAKENHI) grant number 22134006 and the Funding Program for World-Leading Innovative Research and Development on Science and Technology (FIRST Program). Data for exome sequencing, as well as SNP array analysis, are found in the European Genome-phenome Archive (EGA) under accession EGAS00001000661. Author contributions: Y.Sa., S.Ma., K.Y., Y.N., T.Y., H.S., and A.K. performed library preparation and DNA sequencing. Y.Shira., Y.Shio., K.C., H.T., and S.Mi. were committed to bioinformatics analyses of resequencing data. Y.Sa. and A.S.-O. performed SNP array analysis. Y.Sa., S.Ma., M.S., R.I., K.K., and O.N. performed the functional analyses of PRKACA mutant. T.M., H.K., M.F., and Y.H. provided specimens and were also involved in planning the project. Y.Sa., S.Ma., M.S., R.I., and S.O. generated figures and tables and wrote the manuscript. S.O. led the entire project. All authors participated in the discussion and interpretation of data and results. Y.Sa., S.Ma., M.S., Y.H., and S.O. are inventors on a patent applied for by Kyoto University that covers the inspection method for Cushing's syndrome and biomarker and theraputic agent thereof (2014-37189).

SUPPLEMENTARY MATERIALS

www.sciencemag.org/content/344/6186/917/suppl/DC1
Materials and Methods
Figs. S1 to S13
Tables S1 to S8
References (*21–26*)

17 February 2014; accepted 11 April 2014
10.1126/science.1252328

Recurrent somatic mutations underlie corticotropin-independent Cushing's syndrome

Yusuke Sato *et al.*

Science **344**, 917 (2014);
DOI: 10.1126/science.1252328

bjh short report

ATF7IP as a novel *PDGFRB* fusion partner in acute lymphoblastic leukaemia in children

Kenichiro Kobayashi,[1] Kazumasa Mitsui,[2] Hitoshi Ichikawa,[3] Kazuhiko Nakabayashi,[4] Masaki Matsuoka,[2] Yasuko Kojima,[2] Hiroyuki Takahashi,[2] Kazutoshi Iijima,[1] Kaori Ootsubo,[5] Keisuke Oboki,[6] Hajime Okita,[1] Kazuki Yasuda,[7] Hiromi Sakamoto,[3] Kenichiro Hata,[4] Teruhiko Yoshida,[3] Kenji Matsumoto,[8] Nobutaka Kiyokawa[1] and Akira Ohara[2]

[1]Department of Paediatric Haematology and Oncology Research, National Research Institute for Child Health and Development, [2]Department of Paediatrics, Toho Omori Medical Centre, [3]Division of Genetics, National Cancer Centre Research Institute, [4]Department of Maternal-Fetal Biology, National Research Institute for Child Health and Development, [5]SRL Inc., Centre for Molecular Biology and Cytogenetics, [6]Department of Molecular Medical Research, Tokyo Metropolitan Institute of Medical Science, [7]Department of Metabolic Disorder, Diabetes Research Centre, National Centre for Global Health and Medicine, and [8]Department of Allergy and Immunology, National Research Institute for Child Health and Development, Tokyo, Japan

Received 22 December 2013; accepted for publication 29 January 2014

Correspondence: Kenichiro Kobayashi, MD, PhD, Department of Paediatric Haematology and Oncology Research, National Research Institute for Child Health and Development, 2-10-1, Okura, Setagaya-ku, Tokyo 157-8535, Japan.
E-mail: kobayashi-kn@ncchd.go.jp

Summary

We identified *ATF7IP* as a novel *PDGFRB* fusion partner in B-progenitor acute lymphoblastic leukaemia (B-ALL) and showed that B-ALL with *ATF7IP/PDGFRB* translocation is included within the genomic lesions of a Philadelphia chromosome (Ph)-like ALL subgroup. Comprehensive analyses of previous repositories of gene expression data sets disclosed that B-ALL cases with high *PDGFRB* expression level in the context of the Ph-like ALL gene are likely to have a *PDGFRB* translocation. Thus, it is possible that measurement of the *PDGFRB* expression level can be utilized as a screening test for the detection of the cryptic *PDGFRB* translocation, especially within the Ph-like ALL subgroup.

Keywords: *PDGFRB*, *ATF7IP*, acute lymphoblastic leukaemia, Ph-like, screening.

The *PDGFRB* gene (located in 5q33) is a frequent target of chromosomal translocation in a broad spectrum of haematological malignancies, and myeloid neoplasm patients with *PDGFR* translocation are now grouped into a distinct clinical entity of the World Health Organization classification: myeloid neoplasm associated with eosinophilia and *PDGFRA* or *PDGFRB* rearrangement (Tefferi & Vardiman, 2008). Despite increasing evidence of *PDGFR* translocations in haematological malignancy, little is known about *PDGFRB* involvement in B-progenitor acute lymphoblastic leukaemia (B-ALL), presumably due to the limitation of the detection of cryptic *PDGFRB* translocation with conventional diagnostic procedures. Current advances in RNA sequence analysis of B-ALL identified a novel fusion chimera involving *PDGFRB* in

 doi:10.1111/bjh.12834

high-risk B-ALL, namely Philadelphia Chromosome (Ph)-like ALL (Roberts *et al*, 2012). Herein, we report an 8-year-old boy with B-ALL in whom *ATF7IP* was identified as a novel fusion partner in the *PDGFRB* translocation. We examined the molecular characteristics of B-ALL with *PDGFRB* translocation in comparison with previous repositories of gene expression data regarding paediatric B-ALL (Yeoh *et al*, 2002; Roberts *et al*, 2012), and also ascertained that the measurement of *PDGFRB* mRNA expression should be included as a screening test for the detection of such cryptic cytogenetic changes in particular subtypes of ALL, especially Ph-like ALL.

An 8-year-old boy presented in February 2011 with general fatigue of 2 months duration. Physical examination was normal except for pallor and mild hepatomegaly. Laboratory examination showed haemoglobin 47 g/l, platelet count $13{\cdot}1 \times 10^{10}$/l, and leucocyte count $4{\cdot}9 \times 10^{9}$/l (band forms: 30%, segmented neutrophils: 27%, monocytes: 4%, lymphocytes: 23%, and blasts: 16%). A bone marrow (BM) aspirate showed 95% blast cells that stained positive for CD10, CD19, HLA-DR and TdT, but not for myeloperoxidase. Based on these findings, the type of leukaemia of the patient was classified as standard risk B-ALL and he was treated with conventional chemotherapy according to the standard arm of the Tokyo Children's Cancer Study Group Study L99-15 protocol (Manabe *et al*, 2008). He showed good clinical and haematological response with 7 d of prednisolone monotherapy (60 mg/m^2), and blast cells had disappeared from the peripheral blood film on day 8. At the initial diagnosis, a karyotype analysis of blast cells disclosed 45, XY, -7, add (12)(p13). The chromosomal changes involving 12p13 suggested the possibility of t (12;21)(p13;q22); *ETV6/RUNX1* (previously termed *TEL/AML1*), which is known to be the most common translocation in paediatric B-lALL (Jamil *et al*, 2000). The translocation, however, was not detected by either reverse transcription polymerase chain reaction (RT-PCR) or fluorescence *in situ* hybridization (FISH) analysis. Given that the gene locus at 12p13 is frequently involved in chromosomal translocations other than *ETV6*, we performed mRNA sequence analysis (McPherson *et al*, 2011) and identified an in-frame transcript fusing exon 13 of *ATF7IP* with exon 11 of *PDGFRB* (Fig 1A, B). FISH analysis showed cryptic t(5;12)(q33;p13), in which a *ETV6* Dual colour probe (12p13) was fused with a split 3′*PDGFRB* probe (5q33) with a 2-Mb gap (Fig 1C). We also evaluated DNA copy number changes by multiplex ligation-dependent probe amplification analysis (SALSA MLPA KIT P335-A3, MRC-Holland, Amsterdam, the Netherlands), focusing on the common genetic alterations in B-ALL within the *SOX* region, *CRLF2, IKZF1, IL3RA, EBF1, CDKN2A/B, ETV6, BTG1,* and *RB1*. As far as we could determine, no significant copy number alterations except heterozygous deletions within chromosome 7 were present (data not shown). The fusion transcript was readily detected in a BM specimen by quantitative RT-PCR analysis at the time of admission, but its expression decreased with the continuation of chemotherapy. The patient has remained free of disease for 24 months, with the disappearance of the *ATF7IP/PDGFRB* transcripts at the time of this report (Fig 1D, E). To the best of our knowledge, this is the first report showing *ATF7IP* as a fusion partner of *PDGFRB* translocation in haematological malignancy.

ATF7IP has been identified to mediate methylated DNA-binding domain protein 1 (MBD1)-dependent transcriptional repression, recruiting complexes containing SET domain bifurcated 1 (SETDB1) (Fujita *et al*, 2003). Interestingly, a recent analysis suggested that *ATF7IP* facilitates *TERT* and *TERC* expression and is frequently overexpressed in cancer cells (Liu *et al*, 2009). As the N-terminal domain of *ATF7IP* lacked the MBD1 domain, it is likely that the fusion protein does not induce deregulation of *ATF7IP*-mediated transcriptional regulation, but rather is involved in the activation of tyrosine kinase signalling. Indeed, the fusion protein coding ATF7IP locus is predicted to contain a coiled coil structure that is known to contribute to the constitutive activation of kinase and cytokine receptor signalling in *PDGFRB* translocated leukaemia (Lupas *et al*, 1991; Ross & Gilliland, 1999). It is particularly noted that *ATF7IP* fused with *PRGFRB* exon 11, which is the same break point as that of previously reported Ph-like ALL cases with *EBF1/PDGFRB* translocation (Roberts *et al*, 2012).

Fig 1. Detection of *ATF7IP/PDGFRB* fusion gene. (A) Electropherogram of the transcript fusion sequence disclosed in-frame transcript fusing exon 13 of *ATF7IP* with exon 11 of *PDGFRB*. (B) A schematic diagram of the structure of *ATF7IP, PDGFRB,* and novel *ATF7IP-PDGFRB* fusion genes. The arrows indicate the breakpoints. Abbreviations: SETB1, SET domain bifurcated 1; MBD1, methylated DNA-binding domain protein 1; Ig, Immunoglobulin-like domain; TM, transmembrane region; TK, tyrosine kinase domain. (C) Fluorescence *in situ* hybridization (FISH) analysis showing chromosomal change of t (5;12)(q33;p13). Signal detection was carried out on metaphases according to the manufacturer's protocols with the following probes: *PDGFRB* Break (KI-10004 KREATECH) and *ETV6* Dual colour Break Apart Rearranged Probe (Vysis Abbott Molecular, Abbot Park, IL). Left upper panel: *PDGFRB* translocation was represented with split signals of 5′*PDGFRB* (broad green arrow) and 3′*PDGFRB* (broad red arrow), respectively. We used *ETV6* Dual colour probes to depict an *ATF7IP* locus, which is located at approximately 2 Mb centromeric from the *ETV6* loci. The resultant translocation of *ATF7IP/PDGFRB* developed fused signals with *ETV6* Dual colour signals (large arrowhead) and 3′*PDGFRB* (broad red arrow) with a 2-Mb gap. Right upper panel: The FITC filter discriminates the presence of split 5′*PDGFRB* (broad green arrow) and the Non-split *PDGFRB* (arrow), respectively. Scale bar, 2 Mb. Bottom: Genomic view of chromosome 12p13 from the UCSC genome Bioinformatics showing the loci of *ETV6* and *ATF7IP*, respectively. (D) Clinical course of the patient with a longitudinal monitoring of the fusion transcript. Top: Percentage of blast cells in a bone marrow specimen. Bottom: The *ATF7IP/PDGFRB* mRNA level was determined by quantitative reverse transcription polymerase chain reaction (RT-PCR). The expression levels were normalized with *ACTB* before calculating the expression ratios. N.D.: the chimeric mRNA was no longer detectable on day 540. (E) RT-PCR analysis of the expression of the *ATF7IP/PDGFRB* fusion transcript (81 bp). *ACTB* confirms the integrity of cDNA (100 bp). Lane 1–2 at diagnosis; lane 3–4 at day 540.

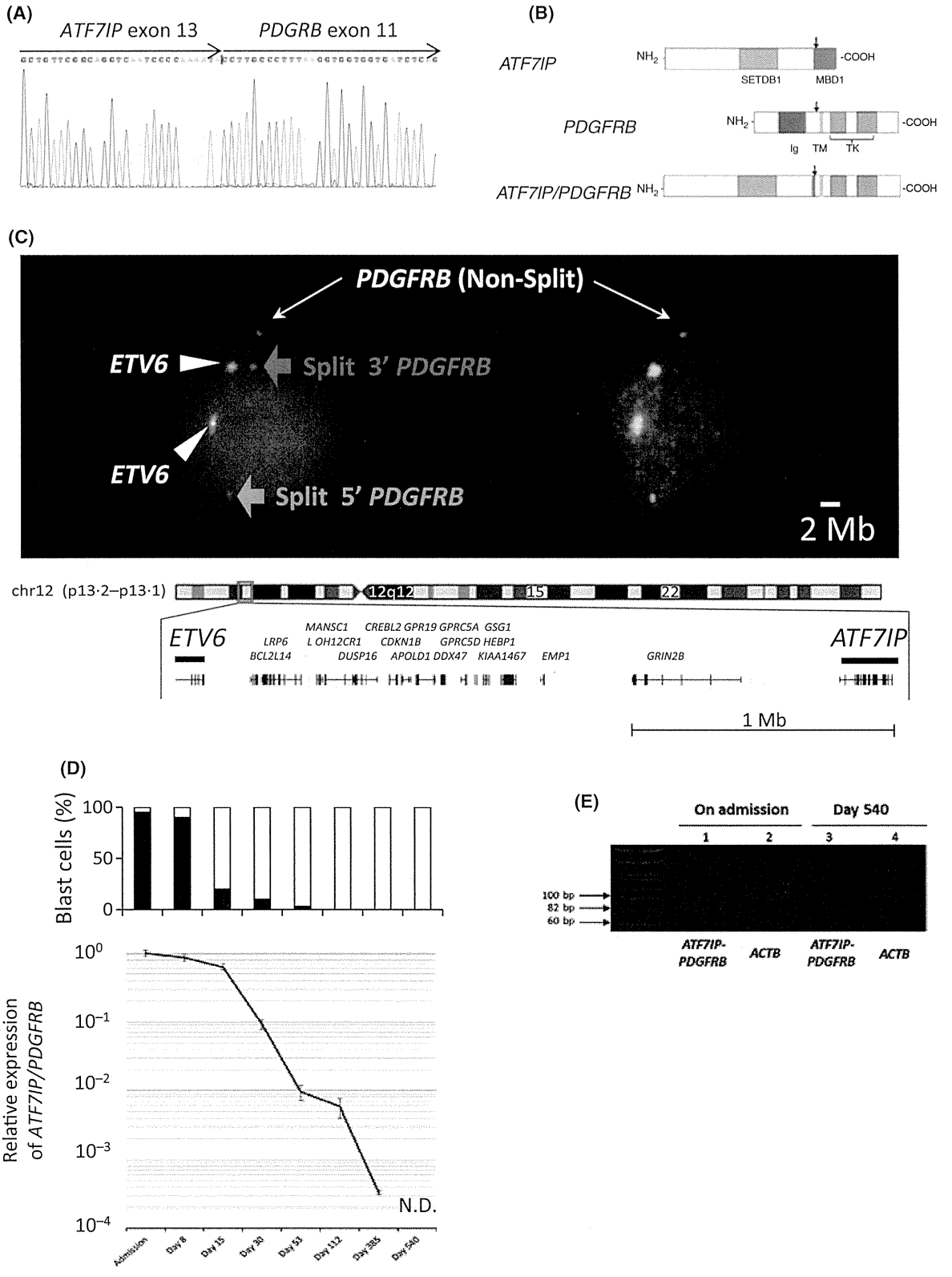

It is strongly suggested that *PDGFRB* translocation in B-ALL comprises a distinct clinical entity, as was shown in acute myeloid leukaemia (Tefferi & Vardiman, 2008). Therefore, we performed microarray analysis of a BM specimen obtained at the time of admission, and compared its expression profiles with public repositories of expression data sets of B-ALL with *BCR-ABL1* translocation (16 cases) and B-ALL without recurrent chromosomal changes (19 cases) (Yeoh *et al*, 2002). By employing gene set enrichment analysis (GSEA) (Subramanian *et al*, 2007), significant enrichment of the *BCR-ABL1* gene expression signature was demonstrated in our case, indicating that B-ALL with *ATF7IP/PDGFRB* translocation can be classified as Ph-like ALL (Fig 2A, B). Interestingly, we found that our case of *ATF7IP/PDGFRB* translocation showed high expression of *PDGFRB* at the mRNA level (Fig 2C). This observation prompted us

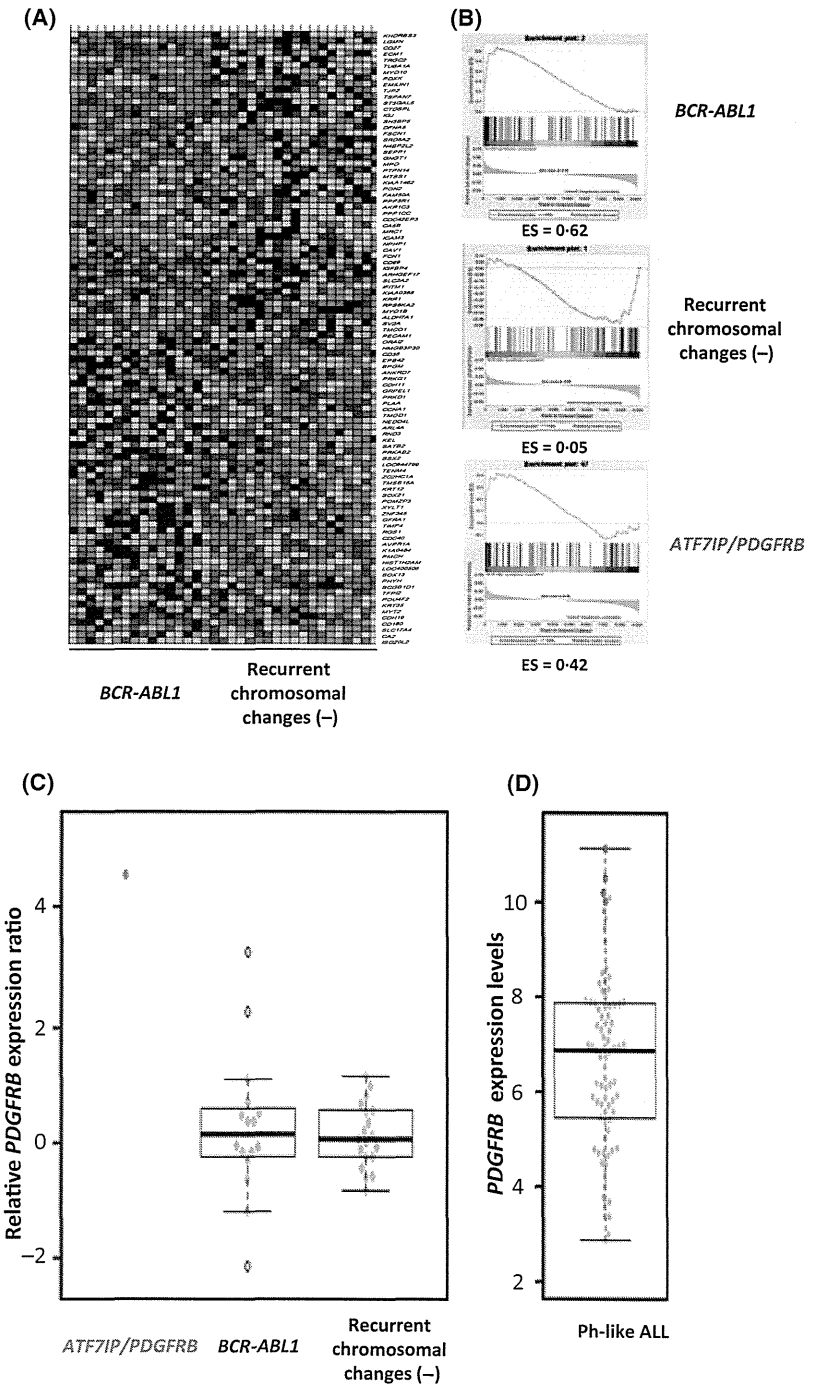

Fig 2. Characterization of gene expression profiles of B-ALL cases with *PDGFRB* translocation. (A–C) Microarray analyses of B-ALL cases with translocation of *ATF7IP/PDGFRB*, *BCR-ABL1* and B-ALL cases without recurrent chromosomal changes. Microarray data set of *ATF7IP/PDGFRB* was obtained from a bone marrow specimen at the time of admission. Expression data sets of both *BCR-ABL1* translocated B-ALL and B-ALL without recurrent chromosomal changes were obtained from those reported by Yeoh *et al* (2002). (A) The top 50 probe sets differentially expressed between *BCR-ABL1* translocated B-ALL and B-ALL without recurrent chromosomal changes are presented as a heat map. (B) Representative GSEA plots of the each subtype of B-ALL i.e. B-ALL with translocation of *BCR-ABL1*, B-ALL without recurrent chromosomal changes and *ATF7IP/PDGFRB* are shown. The enrichment score (ES) is shown at the bottom of the graph. (C) Distribution of the *PDGFRB* expression in B-ALL patients. The expression levels were normalized with *GAPDH* and calculated as the relative *PDGFRB* expression ratio. The ratio in each patient was represented as bee-swarm plots with boxplots. Horizontal bars, median; box, 25–75th percentile; error bars, 10–90th percentile. (D) Distribution of the *PDGFRB* expression within Ph-like ALL patients. Expression data were obtained from the high-risk ALL cohort data set from Children's oncology group (Roberts *et al*, 2012). Four patients with *EBF1/PDGFRB* translocation are indicated as red plots. Data presentation and analyses were performed as in Fig 2C.

to evaluate another data set of 83 cases of Ph-like ALL (Roberts *et al*, 2012), and found that four cases of *EBF1/PDGFRB* translocation also overexpressed *PDGFRB* (Fig 2D). It is noteworthy that Erben *et al* (2010) reported that screening of *PDGFRA or PDGFRB* translocation is facilitated by quantification of *PDGFRA or PDGFRB* expression in eosinophilia-associated myeloproliferative neoplasms (Erben *et al*, 2010). More importantly, *PDGFRB* overexpression was found in patients with diverse *PDGFRB* translocations irrespective of the fusion partner, i.e. *ETV6-PDGFRB, CCDC6-PDGFRB, GIT2-PDGFRB, MYO18A-PDGFRB and SART3-PDGFRB.* Indeed, precise detection of *PDGFRB* translocations is necessary for not only diagnostic purposes but also for providing tailored therapy, such as tyrosine kinase inhibitor (TKI) treatment (Roberts *et al*, 2012). However, the *PDGFRB* translocation is mostly cryptic and it is difficult to detect with conventional cytogenetic studies, as was shown in our case. We speculate that this might be one of the leading causes of the previous poor recognition of *PDGFRB* translocation in paediatric B-ALL. In view of the limited conventional diagnostic procedures for the detection of *PDGFRB* translocation, we speculate that the quantification of the *PDGFRB* mRNA expression level should be utilized as a simple screening test prior to performing or planning microarray-based comparative genomic hybridization or FISH analysis of the *PDGFRB* locus in specific subtypes of B-ALL, especially in the Ph-like ALL subgroup.

In summary, we have identified *ATF7IP* as a novel fusion partner in *PDGFRB* translocation in a paediatric case of B-ALL. Given the potential suitability of TKI treatment in this particular type of B-ALL (Roberts *et al*, 2012; Lengline *et al*, 2013; Weston *et al*, 2013), detection of cryptic *PDGFRB* translocation is important, especially for patients who would benefit from TKI treatment at the correct clinical phases. Thus, we ascertained the future prospective of measuring *PDGFRB* expression levels as a simple screening test to detect cryptic *PDGFRB* translocation especially in the Ph-like ALL subgroup.

Acknowledgements

This work was supported in part by a Health and Labour Sciences Research Grant (3rd-term comprehensive 10-year strategy for cancer control H22-011), the Grant of the National Centre for Child Health and Development (25-2, 24-16), and the Advanced Research for Medical Products Mining Programme of the National Institute of Biomedical Innovation (NIBIO, 10-41, -42, -43, -44, -45).

Author contributions

K.K. analysed results and wrote the manuscript; K.M., M.M., Y.K., H.T., K.I. analysed results; K.O. performed FISH analyses; H.I., N.K., K.I., K.Y., H.S., K.H., K.M. provided informatics support; T.Y., N.K., A.O. designed the research.

Competing interests

The authors have no competing interests.

References

Erben, P., Gosenca, D., Muller, M.C., Reinhard, J., Score, J., Del Valle, F., Walz, C., Mix, J., Metzgeroth, G., Ernst, T., Haferlach, C., Cross, N.C., Hochhaus, A. & Reiter, A. (2010) Screening for diverse PDGFRA or PDGFRB fusion genes is facilitated by generic quantitative reverse transcriptase polymerase chain reaction analysis. *Haematologica*, **95**, 738–744.

Fujita, N., Watanabe, S., Ichimura, T., Ohkuma, Y., Chiba, T., Saya, H. & Nakao, M. (2003) MCAF mediates MBD1-dependent transcriptional repression. *Molecular and Cellular Biology*, **23**, 2834–2843.

Jamil, A., Theil, K.S., Kahwash, S., Ruymann, F.B. & Klopfenstein, K.J. (2000) TEL/AML-1 fusion gene. its frequency and prognostic significance in childhood acute lymphoblastic leukemia. *Cancer Genetics and Cytogenetics*, **122**, 73–78.

Lengline, E., Beldjord, K., Dombret, H., Soulier, J., Boissel, N. & Clappier, E. (2013) Successful tyrosine kinase inhibitor therapy in a refractory B-cell precursor acute lymphoblastic leukemia with EBF1-PDGFRB fusion. *Haematologica*, **98**, e146–e148.

Liu, L., Ishihara, K., Ichimura, T., Fujita, N., Hino, S., Tomita, S., Watanabe, S., Saitoh, N., Ito, T. & Nakao, M. (2009) MCAF1/AM is involved in Sp1-mediated maintenance of cancer-associated telomerase activity. *The Journal of Biological Chemistry*, **284**, 5165–5174.

Lupas, A., Van Dyke, M. & Stock, J. (1991) Predicting coiled coils from protein sequences. *Science*, **252**, 162–1164.

Manabe, A., Ohara, A., Hasegawa, D., Koh, K., Saito, T., Kiyokawa, N., Kikuchi, A., Takahashi, H., Ikuta, K., Hayashi, Y., Hanada, R. & Tokyo Children's Cancer Study Group (2008) Significance of the complete clearance of peripheral blasts after 7 days of prednisolone treatment in children with acute lymphoblastic leukemia: the Tokyo Children's Cancer Study Group Study L99-15. *Haematologica*, **93**, 1155–1160.

McPherson, A., Hormozdiari, F., Zayed, A., Giuliany, R., Ha, G., Sun, M.G., Griffith, M., Heravi Moussavi, A., Senz, J., Melnyk, N., Pacheco, M., Marra, M.A., Hirst, M., Nielsen, T.O., Sahinalp, S.C., Huntsman, D. & Shah, S.P. (2011) deFuse: an algorithm for gene fusion discovery in tumor RNA-Seq data. *PLOS Computational Biology*, **7**, e1001138.

Roberts, K.G., Morin, R.D., Zhang, J., Hirst, M., Zhao, Y., Su, X., Chen, S.C., Payne-Turner, D., Churchman, M.L., Harvey, R.C., Chen, X., Kasap, C., Yan, C., Becksfort, J., Finney, R.P., Teachey, D.T., Maude, S.L., Tse, K., Moore, R., Jones, S., Mungall, K., Birol, I., Edmonson, M.N., Hu, Y., Buetow, K.E., Chen, I.M., Carroll, W.L., Wei, L., Ma, J., Kleppe, M., Levine, R.L., Garcia-Manero, G., Larsen, E., Shah, N.P., Devidas, M., Reaman, G., Smith, M., Paugh, S.W., Evans, W.E., Grupp, S.A., Jeha, S., Pui, C.H., Gerhard, D.S., Downing, J.R., Willman, C.L., Loh, M., Hunger, S.P., Marra, M.A. & Mulligan, C.G. (2012) Genetic alterations activating kinase and cytokine receptor signaling in high-risk acute lymphoblastic leukemia. *Cancer Cell*, **22**, 153–166.

Ross, T.S. & Gilliland, D.G. (1999) Transforming properties of the Huntingtin interacting protein 1/platelet-derived growth factor beta receptor fusion protein. *The Journal of Biological Chemistry*, **274**, 22328–22336.

Subramanian, A., Kuehn, H., Gould, J., Tamayo, P. & Mesirov, J.P. (2007) GSEA-P: a desktop application for gene set enrichment analysis. *Bioinformatics*, **23**, 3251–3253.

Tefferi, A. & Vardiman, J.W. (2008) Classification and diagnosis of myeloproliferative neoplasms: the 2008 World Health Organization criteria and point-of-care diagnostic algorithms. *Leukemia*, **22**, 14–22.

Weston, B.W., Hayden, M.A., Roberts, K.G., Bowyer, S., Hsu, J., Fedoriw, G., Rao, K.W. & Mullighan, C.G. (2013) Tyrosine kinase inhibitor therapy induces remission in a patient with refractory EBF1-PDGFRB-positive acute lymphoblastic leukemia. *Journal of Clinical Oncology*, **31**, e413–e416.

Yeoh, E.J., Ross, M.E., Shurtleff, S.A., Williams, W.K., Patel, D., Mahfouz, R., Behm, F.G., Raimondi, S.C., Relling, M.V., Patel, A., Cheng, C., Campana, D., Wilkins, D., Zhou, X., Li, J., Liu, H., Pui, C.H., Evans, W.E., Naeve, C., Wong, L. & Downing, J.R. (2002) Classification, subtype discovery, and prediction of outcome in pediatric acute lymphoblastic leukemia by gene expression profiling. *Cancer Cell*, **1**, 133–143.

Int J Hematol (2014) 100:180–187
DOI 10.1007/s12185-014-1622-y

ORIGINAL ARTICLE

Treatment outcomes of adolescent acute lymphoblastic leukemia treated on Tokyo Children's Cancer Study Group (TCCSG) clinical trials

Motohiro Kato · Atsushi Manabe · Katsuyoshi Koh · Takeshi Inukai · Nobutaka Kiyokawa · Takashi Fukushima · Hiroaki Goto · Daisuke Hasegawa · Chitose Ogawa · Kazutoshi Koike · Setsuo Ota · Yasushi Noguchi · Akira Kikuchi · Masahiro Tsuchida · Akira Ohara

Received: 23 April 2014 / Revised: 11 June 2014 / Accepted: 11 June 2014 / Published online: 18 June 2014

Abstract There is no standard treatment for adolescents aged 15 years or older with acute lymphoblastic leukemia (ALL), although this age group has been reported as having a poorer prognosis compared to younger patients. We retrospectively analyzed the outcomes of three consecutive Tokyo Children's Cancer Study Group ALL trials (1995–2006) of 373 patients aged 10 years or older, with particular focus on adolescents aged 15–18 years (older-adolescents $n = 41$), compared to those aged 10–14 years (younger-adolescents $n = 332$). The probability of event-free survival at 8 years was 67.5 ± 7.4 % for the older-adolescents and 66.5 ± 2.6 % for the younger-adolescents ($p = 0.95$). Overall survival was 70.7 ± 7.1 % for the older-adolescents and 74.3 ± 2.4 % for the younger-adolescents ($p = 0.48$). The differences between groups in relapse incidence, non-relapse mortality, and death rate during induction were not statistically significant, although the older-adolescents trended towards a higher frequency of having stem-cell transplantation during the first remission. In conclusion, our treatment strategy, which consists of intensive induction and block-type consolidation, provided improved outcomes for patients aged 15–18 years, comparable to those for patients aged 10–14 years.

Keywords Acute lymphoblastic leukemia · Adolescents · Clinical trial

Electronic supplementary material The online version of this article (doi:10.1007/s12185-014-1622-y) contains supplementary material, which is available to authorized users.

M. Kato (✉)
Department of Pediatrics, The University of Tokyo, 7-3-1 Hongo, Bunkyo-ku, Tokyo 113-8655, Japan
e-mail: katom-tky@umin.ac.jp

M. Kato
Department of Cell Therapy and Transplantation Medicine, The University of Tokyo, Tokyo, Japan

A. Manabe · D. Hasegawa
Department of Pediatrics, St. Luke's International Hospital, Tokyo, Japan

K. Koh
Department of Hematology/Oncology, Saitama Children's Medical Centre, Saitama, Japan

T. Inukai
Department of Pediatrics, University of Yamanashi, Kofu, Japan

N. Kiyokawa
Department of Pediatric Hematology and Oncology Research, National Research Institute for Child Health and Development, Tokyo, Japan

T. Fukushima
Department of Pediatrics, Tsukuba University, Tsukuba, Japan

H. Goto
Division of Hemato-oncology/Regenerative Medicine, Kanagawa Children's Medical Center, Yokohama, Japan

C. Ogawa
Division of Pediatric Oncology, National Cancer Center Hospital, Tokyo, Japan

K. Koike · M. Tsuchida
Department of Hematology/Oncology, Ibaraki Children's Hospital, Mito, Japan

Introduction

Prognosis of pediatric acute lymphoblastic leukemia (ALL) has dramatically improved and recent clinical studies report excellent results for children [1–7]; however, the probability of survival of older children is unsatisfactory [7, 8]. The biological and molecular genetic features differ between older and younger children with ALL [9–14], such as higher frequency of poor prognostic factors, T-cell phenotype [12], *BCR-ABL1* translocations [14] and a lower frequency of favorable prognostic factors, including high hyperdiploidy and the *ETV6-RUNX1* translocation [13].

Thus, specific attention should be paid for older children with ALL, and pediatric-specific intensive chemotherapy could improve the outcomes of this group [8, 10, 15–19]. Although 15 years or older adolescents have been reported as a risk factor for poor outcome because of higher induction failure, relapse and therapy-related mortality [8, 15, 18, 20], there is limited information available regarding the characteristics of 15 years or older patients with ALL who underwent treatment in clinical studies [8, 11, 19]. Therefore, the optimal treatment for this age group is not established [21]. This situation occurs partly because such patients are treated by adult and pediatric oncologists, even though ALL is relatively uncommon in adolescents and young adults.

In the present study, we retrospectively analyzed the long-term outcomes of with ALL aged 10 years or older (younger-adolescents) who were enrolled in the three consecutive Tokyo Children's Cancer Study Group (TCCSG) ALL treatment protocols between 1995 and 2006. We focused particularly on children aged 15–18 years (older-adolescents).

Patients and methods

Patients

A total of 1,755 newly diagnosed ALL patients aged 1–18 years were enrolled in the TCCSG ALL trials L95-14 [22] (from 1995 to 1999, $n = 597$), L99-15/1502 [23–25] (from 1999 to 2004, $n = 754/254$), and L04-16 (from 2004 to 2006, $n = 150$). All protocols were approved by the institutional review board or equivalent committee at each participating institution. Thirty patients were excluded from this study due to insufficient data related to age. Of the remaining 1725 patients, 373 were aged 10 years or older. The median follow-up period for the 373 patients was 8.8 years.

Risk classification

The risk classification system used in these studies was based on age, leukocyte count at diagnosis, and immunophenotype [22–24]. Risk classification regarding patients 10 years or older is described below. In study L95-14 [22], all patients 10 years of age or older were assigned to a high-risk (HR) group. The indication for allogeneic hematopoietic stem-cell transplantation (HSCT) was a leukocyte count at diagnosis >150000 cells/μl, Ph1, or presence of the *MLL* translocation. Autologous peripheral blood stem-cell transplantation was permitted if an allogeneic HLA-matched donor was unavailable. All HR patients received 18 Gy of cranial irradiation.

In the L99-15/1502 [23–25] and L04-16 studies, upon diagnosis, patients were tentatively assigned to standard risk (SR), intermediate risk (IR), or HR groups. Patients aged 10 years or older with a leucocyte count of <50000 or ≥50000 cells/μl at diagnosis were assigned to IR or HR groups, respectively. For patients with non-T-cell ALL, initial IR patients with prednisolone poor response (PPR ≥1000 blasts/μl in peripheral blood on day 8) were reclassified into the HR group. For T-cell ALL, patients with a very good prednisolone response (VGPR, no blasts in peripheral blood on day 8) were assigned to the IR group and the other patients were assigned to the HR group. Patients with the cytogenetics of Ph1 or 11q23 were assigned to the HR group (Supplementary Figure 1). The indication for allogeneic HSCT was initial HR and PPR of non-T ALL, PPR of T-ALL, Ph1, *MLL* translocation, and failure to enter remission at the end of induction.

Therapies employed in the L95-14, L99-15/1502, and 04-16 studies

The chemotherapy schedule is shown in Supplementary Figure 2 and Tables 1–4. Previous reports provide the details of the treatment regimens of L95-14 [22] and L99-15 [23–25]. From July 2003, the treatment schedule for the HR group of the L99-15 study was amended to that of the L99-1502 study. Berlin–Frankfurt–Münster (BFM)-type block consolidations were administered after induction chemotherapy corresponding to that of the L99-15 study.

S. Ota
Department of Pediatrics, Teikyo University Chiba Medical Center, Ichihara, Japan

Y. Noguchi
Department of Pediatrics, Japanese Red Cross Narita Hospital, Narita, Japan

A. Kikuchi
Department of Pediatrics, Teikyo University, Tokyo, Japan

A. Ohara
Department of Pediatrics, Toho University, Tokyo, Japan

HR1′, HR2′, and HR3′ consolidations of BFM-ALL95 [26] were repeated twice, followed by reinduction and maintenance therapy. Identical chemotherapy treatment schedules were employed by the L04-16 and L99-1502 studies. Patients with leukocyte counts 100000 cells/μl or more received cranial irradiation for prophylaxis with 18 Gy (L95-14 and L99-15/1502) or 12 Gy (L04-16).

Statistical analysis

Fisher's exact test was used to compare differences in the distribution of clinical features among each age group. The duration of event-free survival (EFS) was defined as the time from the initiation of therapy to either treatment failure (relapse, death, or the diagnosis of secondary cancer) or the final day of observation that confirmed the patient was alive. Overall survival (OS) was defined as the time from the initiation of therapy to death from any cause or the time of the last follow-up. The probabilities of EFS and OS were estimated using Kaplan–Meier analysis, and the statistical significance of differences was evaluated using the log-rank test.

Cumulative incidences of relapse were estimated taking into account the competing events of death without relapse and development of a secondary malignancy. To determine the cumulative incidence of non-relapse mortality (NRM), relapse and development of secondary malignancy were considered as competing risk factors. Gray's test was used to assess the statistical significance of age on the cumulative incidences.

Multivariate analysis was performed using the Cox proportional hazard regression model, and the variables considered were patient age groups (younger-adolescents 10–14 years, or older-adolescents 15–18 years), treatment protocols, immunophenotype (T or non-T), initial leukocyte count, and peripheral blast count on day 8. All statistical analyses were performed using the R software 2.13.0 (The R Foundation for Statistical Computing, Vienna, Austria). A 2-sided p value <0.05 was considered statistically significant.

Results

Clinical features of adolescent ALL

Patient characteristics are summarized in Table 1. Compared with patients aged <10 years, older children showed male predominance, high leukocyte count at diagnosis, and increased T-cell phenotype. The frequency

Table 1 Clinical characteristics according to age groups

Characteristics	<10 years	10–14 years	15–18 years	p value
Total (n)	1352	332	41	
Study (n)				0.66
L95-14	461	122	14	
L99-15/1502	777	187	22	
L04-16	114	23	5	
Gender n (%)				0.01
Male	736 (54.6)	206 (62.4)	28 (68.3)	
Female	612 (45.4)	124 (37.6)	13 (31.7)	
WBC at diagnosis n (%)				0.01
<50000 cells/μl	885 (65.7)	202 (60.8)	22 (53.7)	
50000–100000 cells/μl	321 (23.8)	76 (22.9)	10 (24.4)	
≥100000 cells/μl	141 (10.5)	54 (16.3)	9 (22.0)	
Immunophenotype n (%)				<0.001
Non-T	1235 (92.1)	260 (78.8)	32 (78.0)	
T	106 (7.9)	70 (21.2)	9 (22.0)	
CNS status[a] n (%)				0.04
CNS-1	1318 (97.9)	324 (97.6)	37 (90.2)	
CNS-2	15 (1.1)	5 (1.5)	3 (7.3)	
CNS-3	13 (1.0)	3 (0.9)	1 (2.4)	
Cytogenetics[b] n (%)	1214	310	37	
High hyperdiploid[c]	255 (21.0)	25 (8.1)	2 (5.4)	<0.001
BCR-ABL1	28 (2.3)	14 (4.5)	1 (2.7)	0.02
TCF3-PBX1	46 (3.8)	25 (8.1)	3 (8.1)	<0.001

WBC white blood cell, *CNS* central nervous system, *PGR* prednisolone good responder, *PPR* prednisolone poor responder

[a] CNS status was evaluated at day 8 [23]

[b] Cytogenetic data were not available for 138 patients <10 years of age, 22 patients 10–14 years of age, and 4 patients of 15–18 years of age

[c] High hyperdiploid was cytogenetically defined as 51 or more modal chromosome number

Table 2 Treatment outcome

Characteristics	<10 years	10–14 years	15–18 years	p*
Patients (n)	1352	332	41	
PB blast on day 8 n (%)				0.88
No blasts	597 (44.2)	137 (41.3)	16 (39.0)	
1–1000 blasts/μl	619 (45.8)	146 (44.0)	18 (43.9)	
>1000 blasts/μl	129 (9.5)	49 (14.8)	7 (17.1)	
Missing data	7 (0.5)	0 (0.0)	0 (0.0)	
CR at end of induction n (%)	1275 (94.3)	308 (92.7)	38 (92.7)	1.0
HSCT in the first CR n (%)	120 (8.9)	60 (18.1)	13 (31.7)	0.06
Allogeneic HSCT (n)	97	48	11	
Autologous PBSCT (n)	19	12	2	
Missing data	4	0	0	
Relapse n (%)	264 (19.5)	93 (29.8)	9 (24.3)	0.59
Median period from diagnosis to relapse, days	688	409	348	0.83
Site of relapse n (%)				0.37
Isolated BM	180 (68.2)	67 (79.8)	8 (88.9)	
Combined BM	26 (9.8)	5 (6.0)	1 (11.1)	
Isolated extramedullary	47 (17.8)	12 (14.3)	0 (0.0)	
Missing data	11 (4.2)	0 (0.0)	0 (0.0)	
Death n (%)	181 (13.4)	87 (26.2)	11 (26.8)	0.86
Remission status at death n (%)				0.40
Death after relapse	135 (74.6)	72 (82.8)	8 (72.7)	
Death in the first CR	46 (25.4)	15 (17.2)	3 (27.3)	
Second malignancy n (%)	18 (1.3)	4 (1.2)	1 (2.4)	0.44

PB peripheral blood, *CR* complete remission, *HSCT* hematopoietic stem-cell transplantation, *BM* bone marrow

* p value for 10–14 and 15–18 years

of high hyperdiploidy was lower in patients aged 10 years or older, whereas the presence of the *TCF3–PBX1* translocation was more frequent. However, most of the characteristics of patients aged 10 years or older were not statistically different between the younger-adolescents (10–14 years) and the older-adolescents (15–18 years). Median of initial leukocyte count was 11000 (500–874000) in the younger-adolescents and 15300 (600–416500) in the older-adolescents. Immunophenotype distribution was similar between the two groups, and 21.2 % of younger-adolescents and 22.0 % of older-adolescents were T-cell ALL, respectively. Incidence of central nervous system (CNS) invasion at diagnosis (CNS-2 and 3) in the older-adolescents was nearly 10 % and higher than that in the younger-adolescents (2.4 %), with statistical significance ($p = 0.03$).

Outcomes of adolescent ALL

The treatment outcomes are shown in Table 2. Early response to treatment, the number of day 8 blasts in peripheral blood, and induction rate were similar between the younger-adolescents and the older-adolescents. HSCT at the first CR (CR1) was performed for 60 (18.1 %) of 332 (including 48 allogeneic HSCTs) younger-adolescents and for 13 (31.7 %) of 41 (including 11 allogeneic HSCT) older-adolescents ($p = 0.06$), while only 120 (8.9 %) of 1352 patients younger than 10 years underwent HSCT at CR1.

The probability of EFS of the 373 patients aged 10–18 years was 66.5 ± 2.5 %. Although the EFS of adolescents was worse than that of <10 years patients (76.5 ± 1.2 %), the EFS was similar in younger-adolescents (66.4 ± 2.6 %) and older-adolescents (67.5 ± 7.4 %) ($p = 0.96$) (Fig. 1a). There was no statistical difference between the probabilities of OS at 8 years, which was 74.2 ± 2.4 % for younger-adolescents and 70.7 ± 7.1 % for older-adolescents ($p = 0.46$) (Fig. 1b).

No significant difference in EFS was observed between the two age groups: L95-14 cohort (68.1 ± 4.3 % for younger-adolescents and 76.9 ± 11.7 % for older-adolescents, $p = 0.51$), L99-15 cohort (68.7 ± 3.8 % for younger-adolescents and 63.2 ± 11.1 % for older-adolescents, $p = 0.47$), and L99-1502 and L04-16 (57.7 ± 6.6 % for younger-adolescents and 62.5 ± 17.1 % for older-adolescents, $p = 0.73$).

The cumulative incidence of relapse at 8 years was 29.2 ± 2.5 % for patients aged 10–14 years and 25.0 ± 7.0 % for those aged 15–18 years ($p = 0.45$) (Fig. 2a). The distribution of relapse sites was not